



**Politecnico
di Torino**

Politecnico di Torino

Master of Science in Energy and Nuclear Engineering

Academic Year 2021-2022

March 2022

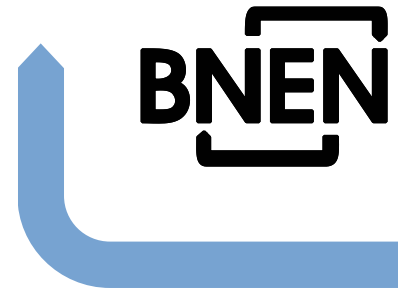
Neutronics modelling of the BR1 reactor with the serpent code

Supervisors:

Dr. Ir. Luca Fiorito (SCK-CEN)
Prof. Subba Fabio (Polito)

Candidate:

Giacomo Caporale



Neutronics modelling of the BR1 reactor with the Serpent code

Giacomo Caporale

Academic year 2020 – 2021

Promotor:

Prof. Dr. Ir Hamid Aït Abderrahim, Université catholique de Louvain

Mentor:

Dr. Ir. Luca Fiorito, SCK•CEN

Co-mentor:

Dr. Ir. Hernandez Solis Augusto, SCK•CEN

Thesis submitted in partial fulfilment of the requirements for the degree of Master of Science in Nuclear Engineering

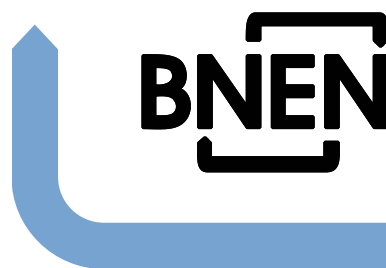


All property right and copy right are reserved. Any communication or reproduction of this document and any communication or use of its contents without explicit authorization is prohibited. Any infringement to this rule is illegal and entitles to claim damages from the infringer, without prejudice to any other right in case of granting a patent of registration in the field or intellectual property.

© BNEN, Belgian Nuclear higher Education Network¹

¹ BNEN is a consortium of the Belgian universities KU Leuven, Université catholique de Louvain (UCL), Université de Liège (ULg), Universiteit Gent (UGent), Vrije Universiteit Brussel (VUB), Université Libre de Bruxelles (ULB) in collaboration with the Belgian Nuclear Research Centre SCK•CEN.
Administration Manager BNEN: Nele Kesteloot c/o SCK•CEN, Boeretang 200, B-2400 MOL, Belgium

Master of Science in Nuclear Engineering



Thesis Summary Page

Name of the student:

Giacomo Caporale

Title:

Neutronics modelling of the BR1 reactor with the Serpent code

Abstract:

BR1 – the first nuclear reactor ever built in Belgium – was critical for the first time on May 11th, 1956. BR1 is air-cooled through a forced convection, moderated by graphite (approximately 500 tons) and fueled with natural metallic uranium. Remarkably, BR1 has used the same original fuel for more than 50 years of operation, and nowadays it has only achieved a burnup of few percent. Years of experience have made this reactor the perfect instrument for fundamental research and training. Existing programs involving instrumentation and data calibration in BR1 require the support of neutronics calculations and an accurate model of the reactor geometry and of the involved particle physics. In the last decade such as support was provided using the MCNP particle transport code.

In this work a detailed model of the BR1 is developed using the Monte Carlo transport code Serpent on the basis of the previous work with MCNP. A comparative analysis is carried out to assess the quality of the new model with respect to experimental data and previous calculations. Added values (or drawbacks) have been identified that the Serpent code can bring to the model in terms of state-of-the-art capabilities, simplifications, computer resource optimization and quality assurance.

Promotor: Prof. Dr. Ir. Hamid Aït Abderrahim, UCL

Mentor: Dr. Ir. Luca Fiorito, SCK•CEN

Co-mentor: Dr. Ir. Hernandez Solis Augusto, SCK•CEN

Assessors: Prof. Dr. Ir. Jean-Marie Noterdaeme, UGent

Prof. Dr. Ir. Maarten Arnst, ULg

Academic Year 2020-2021

Belgian Nuclear higher Education Network, c/o SCK•CEN, Boeretang 200, BE-2400 Mol, Belgium



Acknowledgements

This work closes an important path in my life characterized by many satisfactions and sacrifices. Thanks go to those who gave me the opportunity to carry out this Erasmus project, despite the health emergency. It was a remote activity guaranteed by continuous support from the staff of SCK-CEN. My sincere thanks go to my mentor Dr. Ir. Luca Fiorito who guided me to the realization of the work by providing me with the necessary tools with a serious and professional approach. This has certainly contributed to enriching my academic training. Thanks to my co-mentor Dr. Ir. Hernandez Solis Augusto who suggested and helped me on several occasions, by providing me with useful advice for the project. I thank Prof. Dr. Ir. Hamid Aït Abderrahim, who gave me the opportunity to develop the thesis.

Thanks go to my academic referent and supervisor of the Polytechnic of Turin, Prof. Ir. Fabio Subba for his availability and commitment in following me along this path.

I thank and dedicate the path to my family: my father, mother, brother, grandparents, uncles and all those who have been close to me and who have placed great trust and esteem. They taught me that dedication and passionate can lead to the achievement of great goals.

This career will be the starting point of new experiences that will continue to nurture knowledge and professionalism.

Contents

Acknowledgements.....	i
Contents	ii
List of Figures.....	iv
List of Tables	v
Glossary.....	vi
Introduction.....	8
Chapter 1	9
1.1 Belgian Reactor 1 – BR1.....	9
1.2 Neutron physics	10
1.2.1 Neutron Transport Equation	11
1.2.2 Effective multiplication factor.....	13
1.3 Serpent code.....	16
1.3.1 Nuclear Data Library	17
1.3.2 General aspects on Monte Carlo method.....	17
1.3.3 Basic theorems.....	19
1.4 Other codes	21
1.5 Model verification and validation.....	22
Chapter 2	24
2.1 Geometrical model	24
2.2 Material specification.....	26
2.3 Elementary model	27
2.3.1 Fuel rod	27
2.3.2 Moderator	28
2.3.3 Control rod	31
2.3.4 Biological shielding.....	33
2.4 Source terms	34
2.5 Detectors	34
Chapter 3	35
3.1 Simulation and discussion	35
3.2 Neutronics parameter	35

3.2.1	Output file	35
3.2.2	Results	36
3.3	Power Normalized Factor.....	40
3.4	Reaction rates	41
3.5	Neutron spectra	44
3.6	Neutron flux distribution.....	48
3.7	Power map	51
3.8	Sensitivity analysis	53
3.8.1	Impact of different library	54
3.8.2	Impact of fuel burn up	62
Conclusions		64
References		66

List of Figures

Figure 1. A reduced scale mockup of the BR1 [1].	9
Figure 2. At the left, the generic loading pattern of BR1, where the channels with fuel are filled in black. At the right, a patch of stacked graphite block with the fuel presented as red rods.	10
Figure 3. Schematic representation of the result confidence level.	21
Figure 4. Plane yz with $x = 0$.	24
Figure 5. Plane xz with $y = 0$.	25
Figure 6. Plane xz with $y = 0$.	26
Figure 7. Fuel rod representation. For confidentiality reasons, approximated values are reported.	27
Figure 8. Axial graphite segmentation.	28
Figure 9. Boron 10: comparison of total cross-section and cross-section for (n, alpha) reactions. Source: JANIS (Java-based Nuclear Data Information Software); The JEFF-3.1.1 Nuclear Data Library.	30
Figure 10. Cadmium 113: total cross-section dependent to the energy. Source: JANIS (Java-based Nuclear Data Information Software); The JEFF-3.1 Nuclear Data Library.	31
Figure 11. Control rod model. Figure (a) shows the xz plane view with $y = 135$, (b) the xy plane view with $z = 100$ and (c) the zoom on the xy plane view.	32
Figure 12. Neutron Spectra for channels Y3, Y4, Y5, Y6 and Y7.	45
Figure 13. Elastic cross section of carbon-12. Source: JANIS (Java-based Nuclear Data Information Software); The JEFF-3.1.1 Nuclear Data Library.	46
Figure 14. Neutron Spectra with energy subdivisions.	47
Figure 15. Neutron flux distribution of channel Y3.	49
Figure 16. Neutron flux distribution of channel Y4.	50
Figure 17. Neutron flux distribution of channel Y5.	50
Figure 18. Neutron flux distribution of channel Y6.	50
Figure 19. Neutron flux distribution of channel Y7.	51
Figure 20. Power map of BR1.	52
Figure 21. Relative error of the power factors.	53
Figure 22. Power factors with JEFF 3.2.1 library.	55
Figure 23. Relative error evaluated with JEFF 3.2.1 library.	55
Figure 24. Power factors with JEFF 3.3 library.	57
Figure 25. Relative error evaluated with JEFF 3.3 library.	57
Figure 26. Power factors with JENDL-4.0u library.	59
Figure 27. Relative error evaluated with JENDL-4.0u library.	59
Figure 28. Power factors with ENDF/B-VIII.0 library.	61
Figure 29. Relative error evaluated with ENDF/B-VIII.0 library.	61

List of Tables

Table 1. Fuel rod composition.....	28
Table 2. Graphite isotopic composition.....	29
Table 3. Control rod model isotopic composition.	33
Table 4. Barite concrete isotopic composition.	34
Table 5. Some index of Serpent code output file.	35
Table 6. Neutronics parameters.....	36
Table 7. Precursors group data.	39
Table 8. Reaction rates of U235 and U238.	42
Table 9. Reaction rates of graphite A and graphite B.....	42
Table 10. Reaction rates of cladding.	43
Table 11. Reaction rates of control rod.	43
Table 12. Total neutron flux for each channel.....	48
Table 13. Neutronics parameter with JEFF 3.2.1 library.	54
Table 14. Neutronics parameter with JEFF 3.3 library.	56
Table 15. Neutronics parameter with JENDL-4.0u library.	58
Table 16. Neutronics parameter with ENDF/B-VIII.0 library.	60
Table 17. Comparison between fresh and depleted fuel.....	63

Glossary

ACE:	A Compact ENDF format
BR1:	B elgian R eactor 1
CEA:	Atomic Energy Commission
CLT:	C entral L imit T heorem
CRPG	C omputational R eactor P hysics G roup
CSG:	C onstructive S olid G eometry
DCHAIN-SP:	Code System for Analyzing Decay and Build-up Characteristics of Spallation Products
ENDF:	E valuated N uclear D ata F ile
FENDL-2.1:	F usion E valuated N uclear D ata L ibrary
JAEA:	J apan A tomc E nergy A gency
JANIS:	J Ava-based N uclear D ata I nformation S oftware
JEFF:	J oint E valuated F ission and F usion F ile
KEK:	The High Energy Accelerator Research Organization
LLN:	L aw of L arge N umbers
MCNP:	M onte C arlo N - P articles transport
MIT:	M assachusetts I nstitute of T echnology
NTE:	N eutron T ransport E quation
ORNL:	O ak R idge N ational L aboratory
PF:	P ower F actor
PHITS:	P article and H heavy I on T ransport code S ystem
PNF:	P ower N ormalization F actor
RIST:	R egional I nstitute of S cience & T echnology

SCK•CEN:	StudieCentrum voor K ernenergie • Centre d'Étude de l'énergie N ucléaire
SERMA:	Service d'Etudes des R éacteurs et de M athématiques A ppiquées
VTT:	Technical Research Centre of Finland

Introduction

The Belgium is one of the pioneers in the development of nuclear energy in Europe. The first controlled chain reaction was obtained with the BR1(Belgian Reactor 1) research reactor located at the Belgian Nuclear Research Centre SCK-CEN in Mol. The reactor is particularly suited for neutron physics experiments and industrial applications thanks to its large reactor core, flexible operation and different irradiation facilities. The reactor can be easily started up and shut down that provides a very flexible and stable operation. Together with the good thermalization of the neutrons in the graphite moderator and the variety of irradiation possibilities (e.g. series of irradiation channels, standard neutron and gamma radiation fields...) represent the main advantages of this reactor.

The neutronic calculations of BR1 are performed by the MCNP neutron transport code, one of the most widespread codes in nuclear applications. This is based on Monte Carlo method that provides approximated solutions to mathematical problems through statistical sampling experiments on a computer. It is involved in problems with some probabilistic structure and the capability to solve very complicate problems in efficient way defines the wide use in many scientific applications.

The study wants to characterize and develop another neutron model of the BR1 using Monte Carlo transport code Serpent on the basis of the current model with MCNP. The results obtained from the simulation of the new code will be to compare with experimental data and previous calculations. This is useful to assess the quality and the reliability of the new model identifying the benefits and drawbacks that the Serpent code can bring to the model. It is needed to remark that the model considers the entire fresh nuclear fuel. This is acceptable given that from the begging the power and burnup fuel level of the reactor are particularly low, far from a normal reactor for civil use. Nowadays the reactor is used to perform fundamental research and training activities. Another assumption refers to the different Nuclear Data Library used for Serpent simulation respect to the MCNP model. In our case, it is used the ENDFB-VII.1 library since the JEFF 3.1.1 nuclear data library is not available for Serpent.

The work is divided in three sections. The first section wants to provide some basic information about the BR1 reactor, the neutron physics and the transport code used for the neutronics modelling. In particular, some physical principles underlying the Monte Carlo method and the neutron calculation are reported. The second section describes the model from the geometric and structural composition point of view for the realization of the input code in Serpent. The neutron parameters that characterize the reactor model are addressed in the third section. The analysis provides the reaction rates of the main nuclides, neutron spectra, neutron flux distribution and the power map of the reactor. Finally, a sensitivity analysis was developed to assess the impact of the main assumptions on the simulation results.

Chapter 1

1.1 Belgian Reactor 1 – BR1

The Belgian Reactor 1 (BR1) was the first research reactor built in Belgium. The criticality was achieved in May 11th in 1956 with a nominal power of 4 MW_{th}. The reactor has been operated since the 1950s up to the current days. Nowadays the reactor operates on a daily basis (maximum 7 hours/day) at power levels up to 700 KW_{th}.

The BR1 is moderated by graphite it is cooled by forced air convection. The reactor temperature remains well below 200 °C. The active core extends approximately by 7 m in along every direction. The fuel rods are located in horizontal channels and they consist of natural metallic uranium cylindrical bar coated by an Al-Si alloy containing 88-wt% aluminum.

The graphite matrix is composed by stacking squared-base prismatic blocks, mostly having a dimension of 18x18x72 cm³. These are stacked in such a way as to manage an 18 cm pitch lattice of 829 horizontal channels with 5x5 cm² square diamond shaped cross section at the bottom where the fuel rods are inserted. Inside of the horizontal channels, it can be filled by 23 cylindrical fuel rods lined up one after the other. The dimension of each metallic rod is ~2.5 cm in diameter and ~20.3 cm in length².

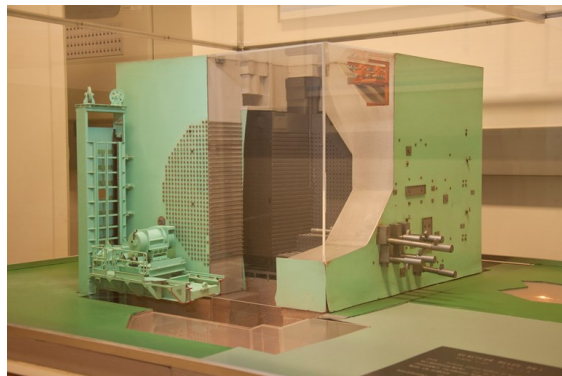


Figure 1. A reduced scale mockup of the BR1 [1].

The loading pattern was changed in the years. Between 1962 and 1975 the loading pattern consisted of 569 fueled channels. Then this configuration was changed since 17 channels have been emptied, leaving 552 fueled channels (Figure 1).

In addition to the fuel rods, there are several channels through the core hosting different instrumentations, regulating control rods and experiments. In particular the reactor has two thermal columns hosting cavity irradiation facilities and 70 channels intended for experimental purposes.

The safety and control of the system is ensured by the safety and control rods that are located in vertical channels. They are divided in six safety rods, five pairs of control rods and two fine regulating rods for the automatic control. These are composed by

² For confidentiality reasons, the values are approximated.

aluminum structural tubes with the inside of this tube made of ~ 2 mm thick layer of cadmium.

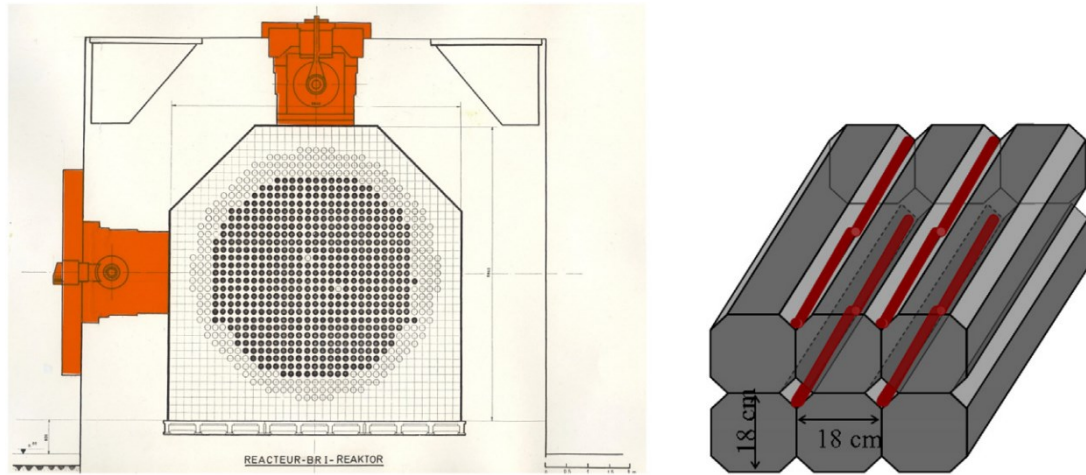


Figure 2. At the left, the generic loading pattern of BR1, where the channels with fuel are filled in black. At the right, a patch of stacked graphite block with the fuel presented as red rods [1].

The BR1 research reactor is characterized by a wide variety of irradiation possibilities, a large reactor core and strong flexibility in its operation. It has different nuclear standard fields, i.e. nuclear radiation fields whose space-, angle- and energy particle flux distribution can be exactly reproduced and ascertained.

The reactor is mainly used as a neutron reference source for reactor physics experiments, neutron activation analysis, and calibration of nuclear detectors and instruments [1].

In addition, there are two thermal columns that hosting cavity irradiation facilities. The vertical column is located at bottom part of the core while the horizontal column is on one side of the core. In the vertical column there is a one meter-diameter cavity in which the neutrons are completely thermalized. They are used as a driver source to obtain specific kinds of standard irradiation fields and for these different converters are loaded in the cavity. The most frequently converters are the so-called MARK-III tube.

1.2 Neutron physics

All simulation codes are based on some fundamental principles that govern the neutron physics. In the following section there are specified some basic concepts

about neutron transport theory starting from the neutron balance equation (NTE) with the different approaches to solve it and the effective multiplication factor.

The main magnitude according to the NTE equation is the neutron angular flux $\phi(\vec{r}, E, \vec{\Omega}, t)$. It is defined as a product between the neutron density n and their speed v :

$$\phi(\vec{r}, E, \vec{\Omega}, t) = n(\vec{r}, E, \vec{\Omega}, t) \cdot v(E) \quad (1.1)$$

The integrate of angular flux over all directions leads to define the scalar neutron flux $\phi(\vec{r}, E, t)$ as follows:

$$\phi(\vec{r}, E, t) = \oint \phi(\vec{r}, E, \vec{\Omega}, t) d\vec{\Omega} \quad (1.2)$$

This is not a constant function because is a dependent variable to the space, time, direction and energy. The neutron flux can be computed by the Serpent code that is based on the Monte Carlo method through different estimators; such as collision estimator, path-length estimator, surface crossing estimator and analytical estimator [2].

1.2.1 Neutron Transport Equation

The NTE is a first-order partial differential-integral equation. It describes the balance statement between neutrons gained and lost according to their interaction. In a simple way, the change on neutron density in time and in a certain volume can be expressed as:

$$\frac{dn}{dt} = Gain - Loss \quad (1.3)$$

Some assumptions are introduced in order to define the neutron transport equation:

- Due to their low density and no charge, the neutron/neutron collisions are considered negligible;
- The collisions between particles are point space and instantaneous;
- For the sake of simplicity, the delayed neutrons contribution is neglected.

Hence, the Boltzmann equation in integra-differential form suited to our system can be defined as follows:

$$\begin{aligned}
\frac{1}{v(E)} \frac{\partial \phi(\bar{r}, E, \bar{\Omega}, t)}{\partial t} + \nabla(\bar{\Omega} \phi(\bar{r}, E, \bar{\Omega}, t)) + \Sigma_t(\bar{r}, E) \phi(\bar{r}, E, \bar{\Omega}, t) = \\
= \iint \Sigma_s(\bar{r}, E') f_s(\bar{r}, E' \rightarrow E, \bar{\Omega}' \rightarrow \bar{\Omega}) \phi(\bar{r}, E', \bar{\Omega}', t) dE' d\bar{\Omega}' \\
+ \iint \bar{v} \Sigma_f(\bar{r}, E') \frac{\chi(\bar{r}, E)}{4\pi} \phi(\bar{r}, E', \bar{\Omega}', t) dE' d\bar{\Omega}'
\end{aligned} \tag{1.4}$$

with \bar{r} is the generic spatial coordinate in cartesian plane, E is the neutron energy according to entire energy spectrum for neutrons, $\bar{\Omega}$ is the flight direction that particles follow after an interaction, t is the time and v is the neutron speed.

Each term has a physical interpretation: the first one defines the time rate of neutrons change in the system considered. The second term is the divergence of the scalar product between the neutron angular flux and the flight direction (i.e. the divergence of the neutron current). It represents the motion of neutrons inside or outside of the phase space of interest. The third term considers all neutrons that after a collision escape from our phase space. In the other side of the Eq.(1.4) there is the scattering term. This accounts the neutrons that belong to another phase space and after the scattering collision they can change the domain and enter in our phase. The fourth and last term represents the generation of the neutrons in our phase space after a fission in the other one.

The neutron angular flux at position \bar{r} , time t , with energy between E and $E + dE$ and direction in the solid angle $d\bar{\Omega}$ about $\bar{\Omega}$ is defined by term $\phi(\bar{r}, E, \bar{\Omega}, t) dE d\bar{\Omega}$. The general quantity $\Sigma(\bar{r}, E)$ represents the macroscopic cross section at \bar{r} for neutrons with energy E . It is related to the probability per unit length that a certain collision (capture, fission, scattering, etc.) happens and it is calculated from the microscopic cross section:

$$\Sigma(\bar{r}, E) = N(\bar{r}) \cdot \sigma(E) \quad \left[\frac{1}{cm} \right] \tag{1.5}$$

With N is the atomic density of the nuclide and σ is the microscopic cross section expressed in $[barn]$ units (equal to $10^{-24} [cm]$) and it represents the effective target area of a single target nucleus for an incident particle.

The nuclear parameter χ is the fission spectrum and it describes the probability that a neutron is emitted at a specific energy after a fission event, in this case at energy E . This depends on the matter and the result energy of neutrons after the process.

The $f_s(\bar{r}, E' \rightarrow E, \bar{\Omega}' \rightarrow \bar{\Omega}) dE d\bar{\Omega}$ is the probability that neutrons leaving a collision with energy between E' and $E' + dE$ and direction in the solid angle $d\bar{\Omega}$ about $\bar{\Omega}'$ given a neutron with the energy E and the direction $\bar{\Omega}$ according to the domain.

Several general features of the equation can be noted. First, it is a linear equation in the unknown dependent variable $\phi(\bar{r}, E, \bar{\Omega}, t)$ with seven independent variables ($\bar{r} \equiv$

$x, y, z; E; \bar{\Omega} \equiv \theta, \varphi; t$). The derivatives in space and in time as well as integrals over angle and energy lead to define as an integrodifferential equation.

However the presence of the derivatives suggest that we must also specify appropriate initial and boundary conditions. In particular the boundary conditions will depend on the particular problem of interest [3].

Below, we briefly describe two different approaches to solve the neutron transport equation: the deterministic and stochastic solution.

1.2.1.1 Deterministic Numerical solution

The first method consists in converting the transport equation into a system of algebraic equations more suitable for a digital computer. This is accomplished by “discretizing” each of the variables in the transport equation, that is, by replacing functions of continuous variables by a discrete set of values at a discrete set of points. The derivatives and integrals appearing in the transport equation must also be replaced by a corresponding discrete representation. In this way, one arrives at a set of algebraic equations for the discrete representation of the dependent variable, the neutron flux ϕ . This discretization can be obtained by using both *discrete ordinates methods* and *function expansions*.

1.2.1.2 Stochastic solution

The second method described to solve the neutron transport equation is based on the probabilistic data. In various scientific and industrial fields, stochastic simulations are taking on a new importance. This is due to the increasing power of computers and the possibilities to simulate more and more complex systems with reduced time consuming. The reference stochastic code is *Monte Carlo method* making use of random sampling to compute the result. The algorithms typically rely on pseudo random numbers, computer generated numbers imitating true random numbers, to generate one possible outcome of a process. All outcomes do not have to be equally probable, and by repeating the procedure with different random numbers as input, one collects data corresponding to the modeled process. On this data, one may then perform a statistical analysis in order to answer different questions about the process [4]. In the Section 1.3 there will be discuss some code that are based on the stochastic method.

1.2.2 Effective multiplication factor

A stable fission chain reaction is necessary to achieve a constant production rate of fission energy in a nuclear system, such as a nuclear reactor. The core must be built in such a way that the rates of neutrons absorption and leakage are balanced by the neutrons born from fissions. In mathematical form it is possible to explain this

balance through the introduction of the multiplication factor concept. A practical definition of the factor can be given in terms of neutron balance relation by defining:

$$k_{eff} \equiv \frac{\text{Number of neutrons produced by fissions}}{\text{Number of neutrons loss in reactor}} \equiv \frac{P(t)}{L(t)} \quad (1.6)$$

The neutrons loss – including absorption and capture reactions – is time dependent, such as the neutrons produced. Both of them phenomena can be described by a production operator P and a loss operator L . In a reactor a multiplication factor $k = 1$ represents an equilibrium condition in terms of neutron population; in this case the system is in a *critical* state. In general:

$$\begin{array}{ll} k_{eff} > 1 & \text{Supercritical system} \\ k_{eff} = 1 & \text{Critical system} \\ k_{eff} < 1 & \text{Subcritical system} \end{array}$$

In the *supercritical system* the number of fission events increases for each neutron generation, hence the chain reaction increases exponentially. In the *subcritical system* the new neutron generation from fissions are too small and the number of neutrons exponentially decrease. The *critical system* is reached when the new neutron generation is equal to the previous one and the chain reaction continue to remain with constant rate. From that, another definition of the effective multiplication factor can be expressed:

$$k_{eff} = \frac{\text{Number of neutrons in one generation}}{\text{Number of neutrons in preceding generation}} \quad (1.7)$$

The neutrons are able to react with the matter in different way but some of them induce fission events that create the new generation of fission neutrons and they contribute to sustain the chain reaction. The Monte Carlo method bases the evaluation of the effective multiplication factor on this definition. The possibility to count the number neutron particles between successive generations leads to obtain an estimate of this neutron parameter.

In order to calculate k_{eff} , it must be evaluated the interaction of neutrons with the matter. Mainly neutrons can be involved in three alternative events: leak out of reactor, be absorbed and scattered by atoms of the materials. In the second case, the absorption can produce a fission reaction if the neutron interaction involves a fissile atom. Otherwise, the neutron is captured without fission and it can produce a transmutation of the atom.

The effective multiplication factor can be rewrite in terms of the most important neutron physical processes that occur in the nuclear reactor. This introduces different factors:

$$k_{eff} = k_{\infty} \cdot P_{NL}^{(th)} \cdot P_{NL}^{(fast)} = \eta \cdot f \cdot p \cdot \varepsilon \cdot P_{NL}^{(th)} \cdot P_{NL}^{(fast)} \quad (1.8)$$

This definition is called six-factor formula and each term is explained.

The first term η is the multiplication factor of the fuel that is identified as the average number of fission neutrons produced per absorption of thermal neutron in the fuel. In general,

$$\eta = \frac{\nu \Sigma_f}{\Sigma_{abs, fuel}} \quad (1.9)$$

The numerical value of η does not change with core temperature for thermal reactor. Moreover, there are small decrease due to the fact there is a continuous reduction in Σ_f^U but on the other hand this decrease is partially compensated by the increase in Σ_f^{Pu} .

The probability factor f is the thermal utilization of the reactor that refers to the ratio of thermal neutron absorptions in the fuel with respect to the total thermal neutron absorptions. In terms of macroscopic cross sections, it can be defined as:

$$f = \frac{\Sigma_{abs, fuel}}{\Sigma_{abs, TOT}} \quad (1.10)$$

This factor will always be less than one since there will be always some thermal neutrons absorbed in the materials different from fuel.

The factor p is called the resonance escape probability and it refers to the fraction of fission neutrons that manage to slow down from fission to thermal energies without being absorbed.

Finally, the fast fission factor ε considers that some fissions will be produced in both fissile and fissionable material by fast neutrons, not only by thermal ones. Hence, it can be expressed in the following form:

$$\varepsilon = \frac{\text{Total number of fission neutrons (from both fast and thermal fission)}}{\text{Number of fission neutrons from thermal fissions}} \quad (1.11)$$

In a thermal reactor the fast fission factor usually has values ranging between $\varepsilon = 1.03$ and $\varepsilon = 1.15$.

These four factors define the multiplication factor in the infinite medium k_{∞} . Here, the possibility to have the leakage of the neutrons is not considered as the infinite domain. Hence, this factor has to be multiplied by the probabilities that fast and thermal neutrons to do not leak from the system, respectively $P_{NL}^{(fast)}$ and $P_{NL}^{(thermal)}$ [5].

1.3 Serpent code

Serpent is a multi-purpose three-dimensional continuous-energy Monte Carlo particle transport code, developed at VTT Technical Research Centre of Finland, Ltd³. The basic geometry description in Serpent relies on a universe-based constructive solid geometry (CSG) model, which allows the description of practically any two- or three-dimensional fuel or reactor configuration. The CSG geometry consists of homogeneous cells filled by different materials, defined by elementary and derived surface types that are combined using logic operators [6].

One of the main advantages of Serpent code is the use of a slightly modified data format. All the isotopes of all materials in the system use the same energy grid. This approach leads to determine the energy grid index only each time the neutron changes its energy. In other methods, each nuclide has a its own energy grid point and every time that the energy index is needed, the code has to repeat an iterative grid search. Despite it is necessary a wide computer memory, the gain is on the efficiency in the computational costs of the calculation [7].

Another important characteristic is related to the Woodcock delta-tracking method that Serpent uses to provide a less expensive computational cost of the simulations. This method will be further discussed later.

³ Ltd: class of private limited company.

1.3.1 Nuclear Data Library

All the nuclear data are produced by the experimental measurements and nuclear model calculations. There is an international collaboration that is regulated through the agreements between the data producers and the users. Once produced, the results have to be collected in the database which includes available experimental values from all the laboratories and then they are managed in a computerized way.

In order to have a better reliability of the available data, they are reviewed due to obsolete methods used or systematic errors. The evaluators make a critical review and gather all experimental information according to the consistency of data processing requirements. The evaluated data files are organized by materials and data types and they are computer readable. The ENDF is the evaluated data files developed in the USA while JEFF is the joint European data files [8].

Serpent reads continuous-energy cross sections from ACE format data libraries [9] [10]. The interaction physics is based on classical collision kinematics and probability table sampling in the unresolved resonance region. ACE format cross section libraries can be derived and processed starting from evaluated nuclear data libraries such as JEF-2.2, JEFF-3.1, JEFF-3.1.1, ENDF/B-VI.8 and ENDFB/B-VII [6].

1.3.2 General aspects on Monte Carlo method

The Monte Carlo code is able to estimate different physical quantities such as flux, current and reaction rates of particles. All of this are quantified as integrated values over the phase space, energy and time that are traduced into space interval (ΔV), energy interval (ΔE), angle ($\Delta \Omega$) and time (Δt).

An integral estimation simplifies noticeable the simulation in terms of computational cost since the point value of certain quantities require a very high accuracy. From this, we can remark that to obtain a simulation with less statistical errors we need to perform a simulation over as higher as possible variables domain. Moreover, the domain that we used to integrate the specific estimator must be compatible to the level of the neutronic settings (i.e. the number of active cycles, the inactive cycle and the neutron source per cycle) [2].

Each simulation consists of a large number of particle histories, in which the random walk of an individual particle is followed, or tracked, through the geometry from its birth to eventual absorption or escape.

The transport simulation follows a random walk from one interaction to the next. The procedure can be described as follows:

- Sample path length (distance to next collision)
- Transport particle to the collision point
- Sample interaction

If the sampled interaction is scattering, the procedure restarts from beginning by sampling the distance to the next collision. The direction and energy are changed in each scattering event.

The neutron path lengths l in the random walk of Monte Carlo simulation are sampled from an exponential distribution using the following definition:

$$l = -\frac{1}{\Sigma_{tot,m}(E)} \ln(\xi) \quad (1.12)$$

Where ξ is a uniformly distributed random variable on the unit interval and $\Sigma_{tot,m}(E)$ is the macroscopic total cross section of material m where the neutron is initially located.

In literature, different techniques exist to perform the particle tallying and evaluate the interested neutron quantities for the MC particle transport problems. The most commonly used are the collision estimator, the path-length estimator, the surface-crossing estimator and analytical estimator. The Serpent code uses the collision estimate of neutron flux [2]. The efficiency of this method results poor if the reaction rates are calculated inside small volumes located in regions of low collision density. However, the use of the collision estimate implies less computational effort directly related in the overall calculation time [11].

Particle transport in Serpent is based on the combination of conventional surface-tracking and the Woodcock delta-tracking method [12] [13] [7].

In general, the interaction probability per traveled path length is given by the macroscopic total cross section and it does not depend on the events that occurred in the particle's history. Therefore, any point in the path can be considered the starting point of a new path. Since the collision probability depends on the material properties, the sampled path length is not statistically valid if the neutron crosses a boundary between two materials. The track has to be stopped at the crossing point and a new path length sampled is defined using the cross section of the next material. This is the general idea in the surface-tracking algorithm.

To stop the particle between two materials, the method needs to evaluate the distance to the nearest boundary surface. This approach is considered the standard tracking algorithm but presents a few drawbacks that appear when it is treated complex geometry:

- In terms of computational cost, the evaluation of the distance to the nearest boundary can be very expensive especially if the cells are included of a large number of surfaces.

- When the mean free path of the particle is large compared to geometry dimensions, stopping the track at each boundary crossing becomes inconvenient from a computational point of view.

To overcome these drawbacks, the alternative algorithm is the Woodcock delta-tracking based on the rejection sampling of particle path lengths. The idea is to effectively homogenize the material total cross sections in such way that the sampled path lengths are valid over the entire geometry. This is accomplished by introducing the concept of a virtual collision, i.e. a scattering reaction that always preserves the neutron energy and direction [6] [14] [15].

1.3.3 Basic theorems

The MC method is based to two fundamental mathematical theorems: Law of Large Numbers (LLN) and the Central Limit Theorem (CLT). Below there is a brief introduction on these concepts.

Suppose we perform a measurement of certain random variable x and that we repeat independently this experiment N times with the same conditions. Hence, we have a collection of random variables:

$$x_1, x_2, x_i, \dots, x_N \quad \text{for } i = 1, 2, \dots, N \quad (1.13)$$

The number of a collection of this random variable defines an independent and identically distributed sequence. At this sequence can be associated a sample average ξ :

$$\xi = \frac{1}{N} \sum_{i=1}^N x_i \quad (1.14)$$

While the expected value $E[x_i]$ and the variance $E[(x_i - E[x_i])^2]$ of the random variables are respectively defined below:

$$E[x_i] = \mu, \quad E[(x_i - E[x_i])^2] = \sigma^2, \quad \text{for } i = 1, 2, \dots, N \quad (1.15)$$

The Law of Large Numbers states that for large number of experiments N the sample average ξ is very close to the expected value with high probability. The mathematical form is expressed as follows:

$$P(|\xi - \mu| \geq k) \leq \frac{\sigma^2}{Nk^2} \quad \text{with } k \in \mathbb{R} \quad (1.16)$$

Where the real number k represents the tolerance of the inequality. Notice that the right-hand side of the statement goes to 0 as $N \rightarrow \infty$. This means that ideally with infinity number of experiments the probability to have the sample average ξ out of the interval $[\mu - k, \mu + k]$ is zero. Moreover, higher it is the real number k (the tolerance) and less it will be the probability [16].

The other important theorem is the Central Limit Theorem. It states that if you have a sample average ξ of certain statistical phenomena and take infinite random samples, the distribution of the sample average will be normally distributed. In mathematical form:

$$\text{for } N \rightarrow \infty$$

$$f_{\xi}(x) = \frac{1}{\sqrt{2\pi \left(\frac{\sigma}{\sqrt{N}}\right)^2}} e^{-\frac{(x-\mu)^2}{2\left(\frac{\sigma}{\sqrt{N}}\right)^2}} \quad (1.17)$$

The Eq. (1.17) shows the normal distribution function of the sample average ξ of the random variable x , which has a mean value μ and standard deviation σ . The number of independent random variables collected is N . The combination of these theorems defines the essence of the Monte Carlo method. When the simulation is performed, many outcomes are collected and they are averaged together to provide an estimate, the sample average. This together with a standard deviation defines a certain error bar, that is the range in which the actual return is present with a specific probability. In particular, the probability that the actual return will be within one standard deviation is 68%, two standard deviation is 95% and three standard deviation is 99.7%. The schematic representation of the confidence level is showed in Figure 3.

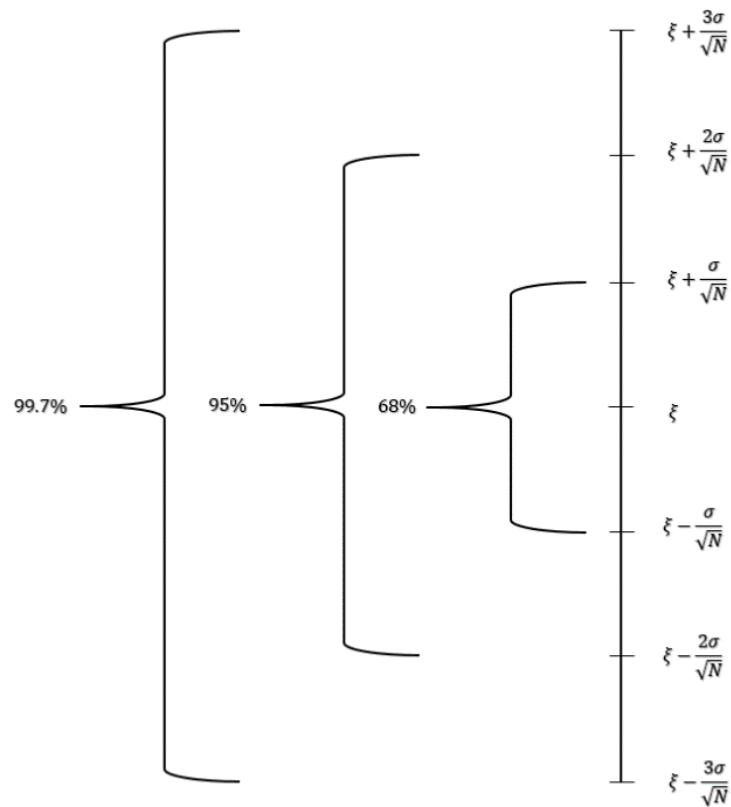


Figure 3. Schematic representation of the result confidence level.

1.4 Other codes

A list of different codes to simulate the neutron transport is presented below. Each of them is based on the Monte Carlo method and they find applications in the nuclear field:

- MCNP (Monte Carlo N-Particle transport) is a MC particle transport code developed at the Los Alamos National Laboratory. It is probably the most widely used transport calculation code. Thanks to wide use and the long history of development, MCNP can be defined as one of the most reliable transport calculation codes. Indeed it is considered the main suitable reference code for Serpent validation. The main neutronics parameters calculated are the multiplication factors, prompt neutron lifetimes, group-wise reaction cross sections and assembly discontinuity factor [7].
- The SCALE/KENO code. The Oak Ridge National Laboratory (ORNL) developed the SCALE, a set of computational tools for criticality safety analysis that is mainly based on two variants of KENO Monte Carlo codes. Both of them perform the effective multiplication factors and the flux

distributions of fissile system in continuous energy and multigroup modes [17].

- The OpenMC code. It is a Monte Carlo particle transport code released for the first time in December 2012. The development was conducted by the Computational Reactor Physics Group (CRPG) at Massachusetts Institute of Technology (MIT). Nowadays, OpenMC is able to simulate only neutrons either in fixed source or k-eigenvalue problems. The data library used is in the ACE format such as having a directed comparison with the other main codes [18].
- PHITS is a Monte Carlo particle transport simulation code developed under collaboration between JAEA, RIST, KEK and several other institutes. Different quantities can be obtained by means of PHITS simulation such as heat deposition, track length and production yields using the implemented “tally” estimator function. Moreover, the PHITS includes the package called DCHAIN-SP that can estimate the time evolution of radioactivity [19] [20].
- TRIPOLI® is the generic name of a Monte Carlo radiation transport codes family dedicated to shielding, reactor physics with depletion, criticality safety and nuclear instrumentation. These were developed by different teams that worked at CEA, e.g. SERMA and DEN. The code TRIPOLI-4® is the reference point of the other codes and it can simulate neutral particles like neutrons and photons with a wide energy range. The nuclear data are readable by TRIPOLI-4® from any evaluation written in ENDF-6 format including JEFF-3.1.1, ENDF/B-VII.1, JENDL-4.0 and FENDL-2.1 libraries [21].

1.5 Model verification and validation

The aim of this project is to provide some bases to involve the Serpent code on the modelling of the BR1 reactor. Any time one wants to introduce a code it is needed to satisfy some guidelines for verifying and validating simulation model. The model is used to predict and perform calculation on the real physical system. It is necessary to know that the model can be used as a substitute for the real system characterizing it through experimentation and analysis. This is the basic concept to define the model sufficient accuracy.

One of the last phases conducted to produce an accurate and credible model are the verification and validation simulation models. The *verification* refers to the processes and techniques that it must be satisfied to demonstrate that the model is based on the right theoretical principles and matches any specifications and assumptions defined. While the *validation* refers to all analysis that assure the accuracy of the representation of the real system, the demonstration that we are building the right model system.

Notice that both the validation and verification are ever completely verified and validated. The model behaviour must be the best approximation of the real system behaviour and when a certain model has been defined validated and verified means that different series of acceptances are carried out to determine the right level of credibility [22] [23].

Chapter 2

2.1 Geometrical model

The Serpent model is based on a text input file with information regarding the system to model. The inputs can be divided as follows:

- The material specification;
- Construction of geometry structure;
- Definition of the location and characteristic of the particle source;
- The desired detector specification to evaluate the final results.

The core geometry is modelled by dividing the entire structure into different elementary module components. In order to create the graphite lattice that accommodates the fuel rods, the simplest way is to focus on each cavity that is built by four graphite blocks. So, this cavity is filled by a single fuel rod element and it is repeated many

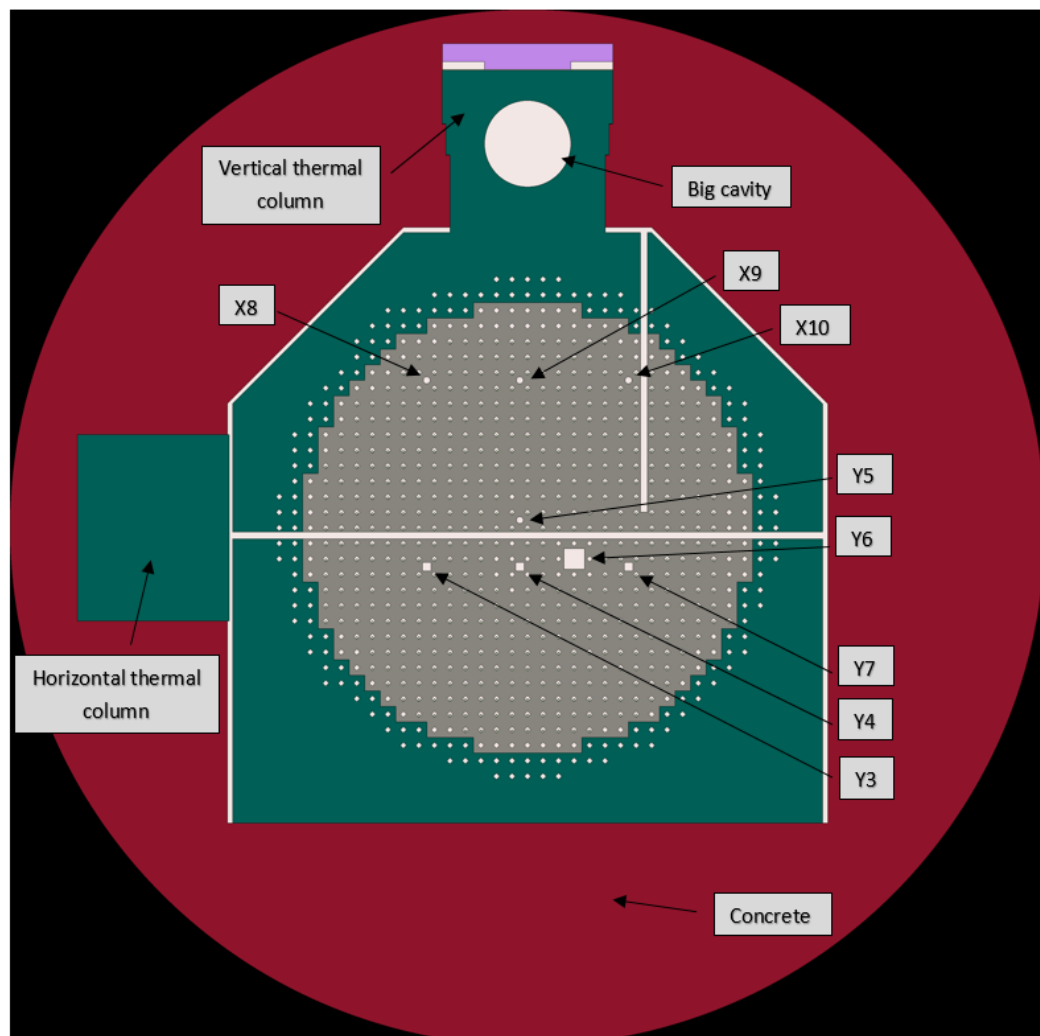


Figure 4. Plane yz with $x = 0$.

times. Moreover, there are different penetrations along the three dimensions in order to accommodate the instrumentations and the control rods. Once the elementary model is defined, the entire core structure is assembled.

Figure 4 shows the front view in the plane yz of the core model from Serpent code. We can see the penetrations parallel to the x-axis, mainly the Y3, Y4, Y5, Y6 and Y7 channels used to characterize some neutronic parameters that will be evaluated.

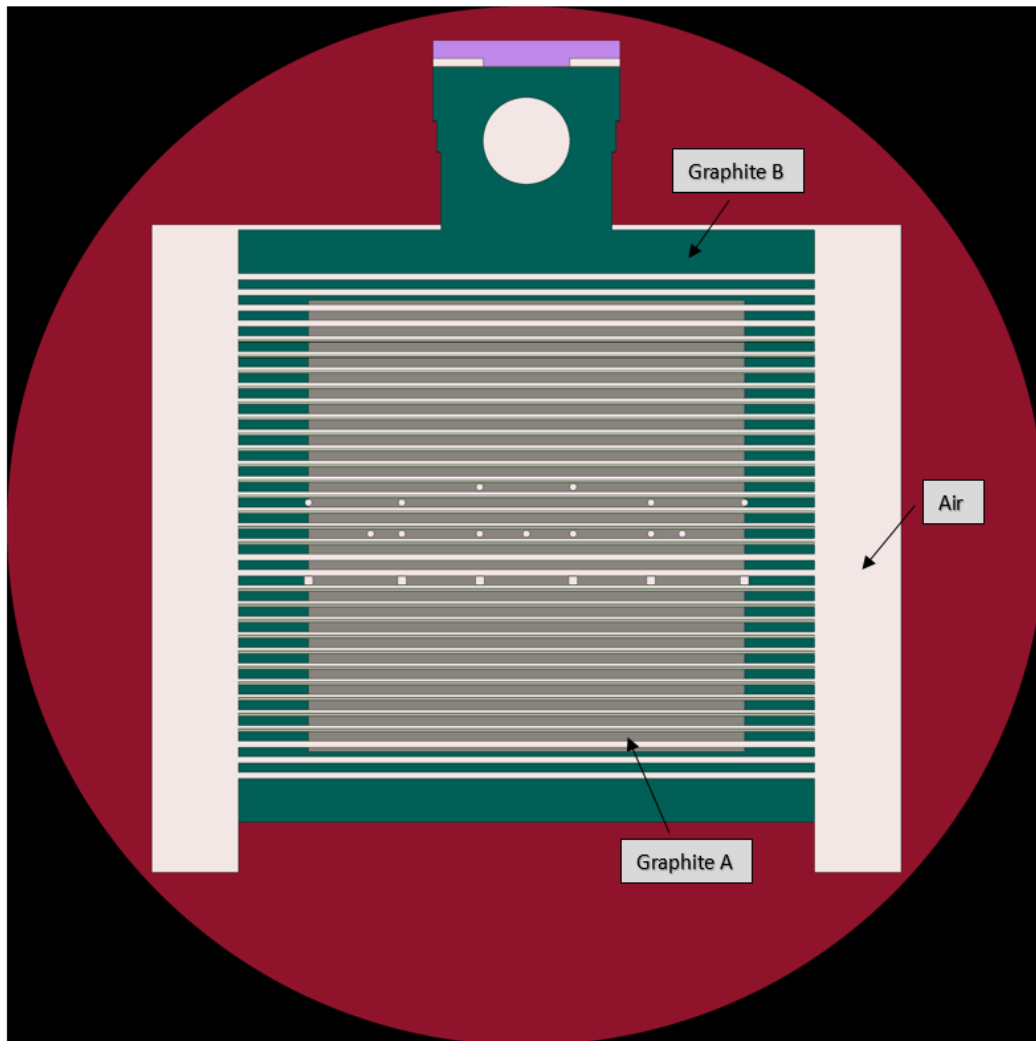


Figure 5. Plane xz with $y = 0$.

Along y-axis there are 13 cylindrical shape penetrations and 6 parallelepiped penetrations used to accommodate the instrumentations. In the Figure 5 we can visualize the air that surrounding the core of the reactor that flows inside the cavity and the different kind of graphite of grade A and B.

The control rods are inserted in vertical way parallel to the z-axis. There are 33 penetrations that provides the accommodation both the control rods and instrumentations. The level of the rod is function of the particular operational condition of the reactor. One example of the plane section normal to the y direction is showed in the Figure 6.

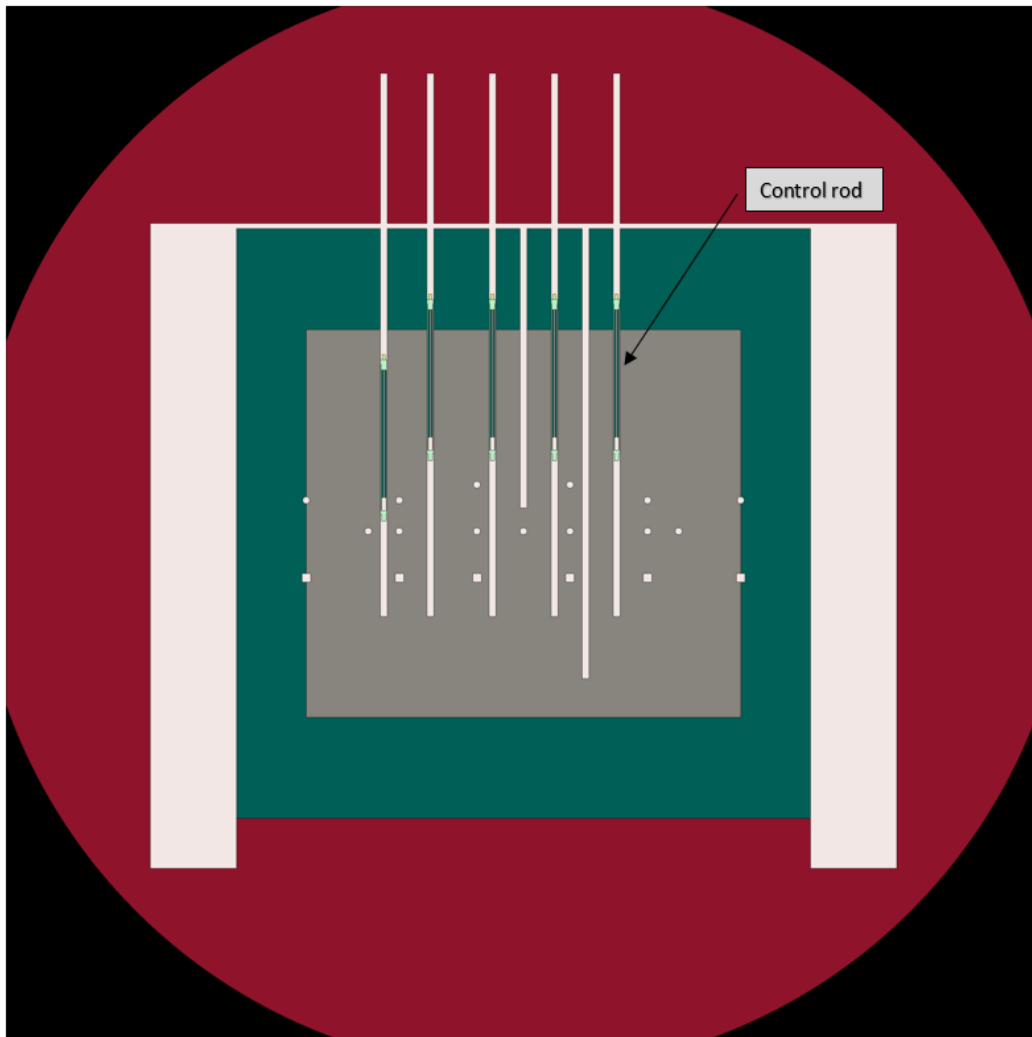


Figure 6. Plane xz with $y = 0$.

2.2 Material specification

In this analysis the nuclear data related to the different materials are based on the ENDF/B-VII.1 library. The main characteristics of this library are an increase in the range amplitude of the neutron cross section, extending from 393 nuclides to 423 nuclides; Modification to thermal neutron reactions on fission products and neutron absorber materials like Cd and Gd; Improved minor actinide evaluations for isotopes of U, Np, Pu and Am [24].

The specific data library (recalled with the command *acelib*) is defined in the input code that contains also the specific files connected to the thermal scattering laws. This phenomenon is important in a reactor that uses graphite as moderator. Since there are thermal neutrons with very low energy, they have the probability to collide with graphite molecules rather than the single carbon atom. The graphite is a crystal and it has some preferential scattering directions that conditions the moderation effect. All these information are considered in the input file introducing the card *therm*.

The materials are evaluated for a temperature at 500 K, the same used for the MCNP simulation of BR1. So the extension *.05c* to recall this information it was added in all materials declaration.

2.3 Elementary model

2.3.1 Fuel rod

The fuel pins are placed in horizontal direction in the many cavities formed by graphite blocks. Each fuel rod is made by an aluminum alloy cladding. Fuel is cooled by air flowing in the cavity. Moreover, for the sake of simplicity the nuclear fuel is considered as single cylindrical material instead of 23 stacked blocks. The fuel is metallic uranium with a natural composition, i.e. the modelled U^{235} enrichment is 0.72 wt%.

Below it is reported a schematic representation of the fuel rod with relative radial dimensions. The graphite surrounds the square while inside it flows the forced air:

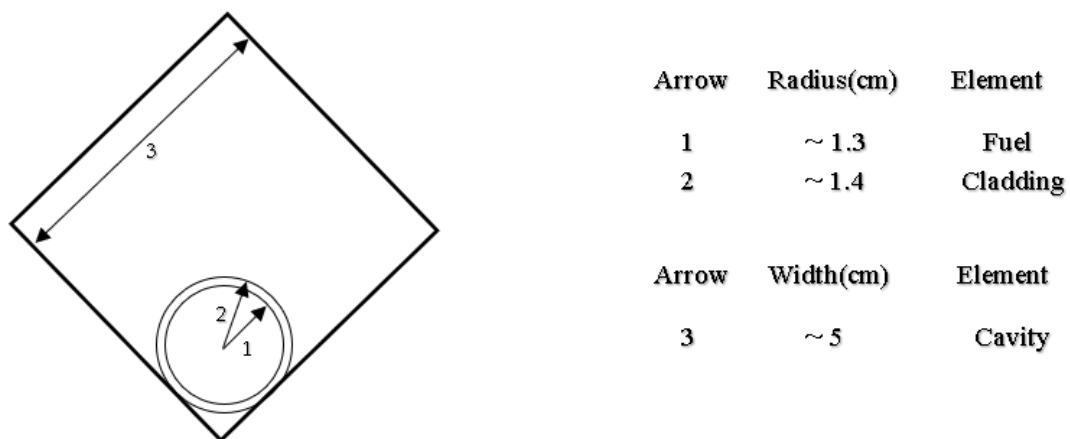


Figure 7. Fuel rod representation. For confidentiality reasons, approximated values are reported.

The material compositions for each fuel rods are showed in the following table:

Material	Composition	Approx. density [g/cm3]
Fuel	U-234, U-238, U-235	18.9
Clad	Al, Si	2.7
Air	C-12, C-13, N-14, O-16, Ar-36, Ar-38, Ar-40	0.0012

Table 1. Fuel rod composition.

2.3.2 Moderator

For the BR1 reactor, the material used to moderate and reflect the neutrons is the graphite. In particular, there are two kinds of graphite: Graphite A and Graphite B. The first has a higher density and a lower impurity content, including boron, whereas the second has lower density and a higher content of impurities. The channels of graphite are different along the axial direction of the core. Above 252 cm, in both direction graphite B is present while within the graphite A is placed. The subdivision is showed in Figure 8 with the relative dimensions:

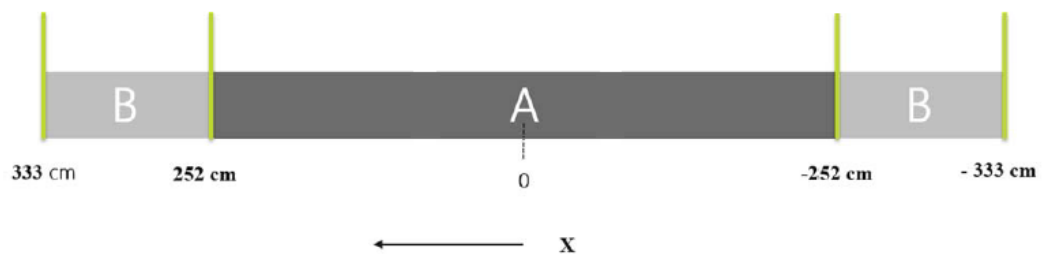


Figure 8. Axial graphite segmentation.

The material composition between the graphite A and B is similar and it is summarized in the following table:

Material	Composition	Approx. density [g/cm3]
Graphite A	C-12, C-13, B-10, B-11	1.7
Graphite B	C-12, C-13, B-10, B-11	1.6

Table 2. Graphite isotopic composition.

The different levels of impurity lead to have diverse capability to absorb the neutron population. Therefore, these atoms tend to capture the neutrons rather than slow down so the efficiency of the moderator decreasing. Since it is important to have a good moderation in centre of core the graphite A with lower impurities is located there. While the graphite B is on the boundary of the core.

In general, in the commercial graphite the impurities can be explained by their natural ‘boron equivalence’, i.e. the boron content which provides the equivalent absorption cross section. In the nuclear field, nuclear grade graphite is defined as having impurities $\leq 5 \text{ ppm}$ boron equivalence [1]. In our case, the concentrations respectively for graphite A and B are 0.38 ppm and 1.6 ppm in weight [1]. Moreover for this study, it is used the fresh graphite composition with the above isotopic composition.

The importance to limit the presence of boron is related to very high capture cross section in the thermal energy region. Below, Figure 9 shows the development of the boron isotope B-10 on the total and capture (n, alpha) cross sections:

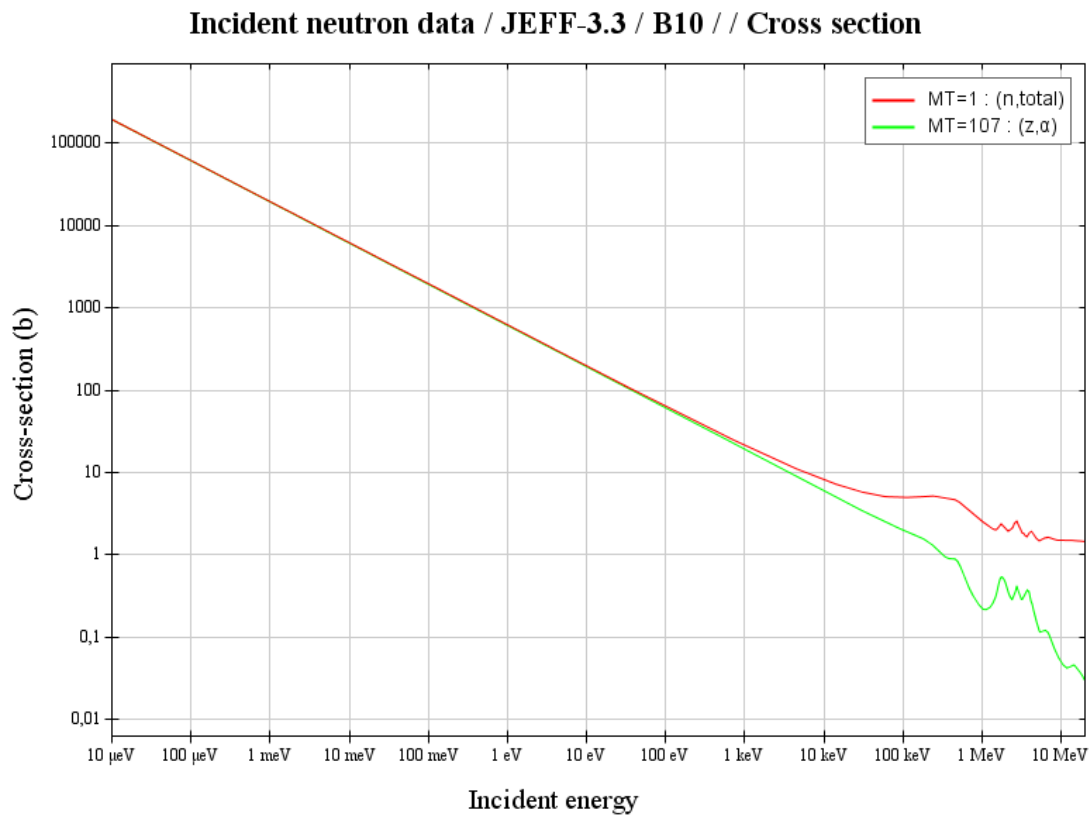


Figure 9. Boron 10: comparison of total cross-section and cross-section for (n, alpha) reactions. Source: JANIS (Java-based Nuclear Data Information Software); The JEFF-3.1.1 Nuclear Data Library.

At 0.025 eV neutron energy the (n, alpha) reaction cross section is about 3800 barns. The high values remain also for fast energy spectrum [25].

2.3.3 Control rod

The vertical penetration of the core (parallel to the z-axis) accommodates both control rods and instrumentation. The cavities that host the control rods are 18 and the level of the insertion is different according to the operation phase of reactor. The control rods structure have the same geometry and composition involving different absorber as cadmium isotopes. The cadmium is an active element used as neutron capture that is included in a thick layer of about 2 mm. This material has a high capture cross section mainly in the thermal region that ensure a good control of the reactor. Below, Figure 10 shows the total cross section of Cd-113, one isotope present in cadmium of the control rod (i.e. 12.22 wt%):

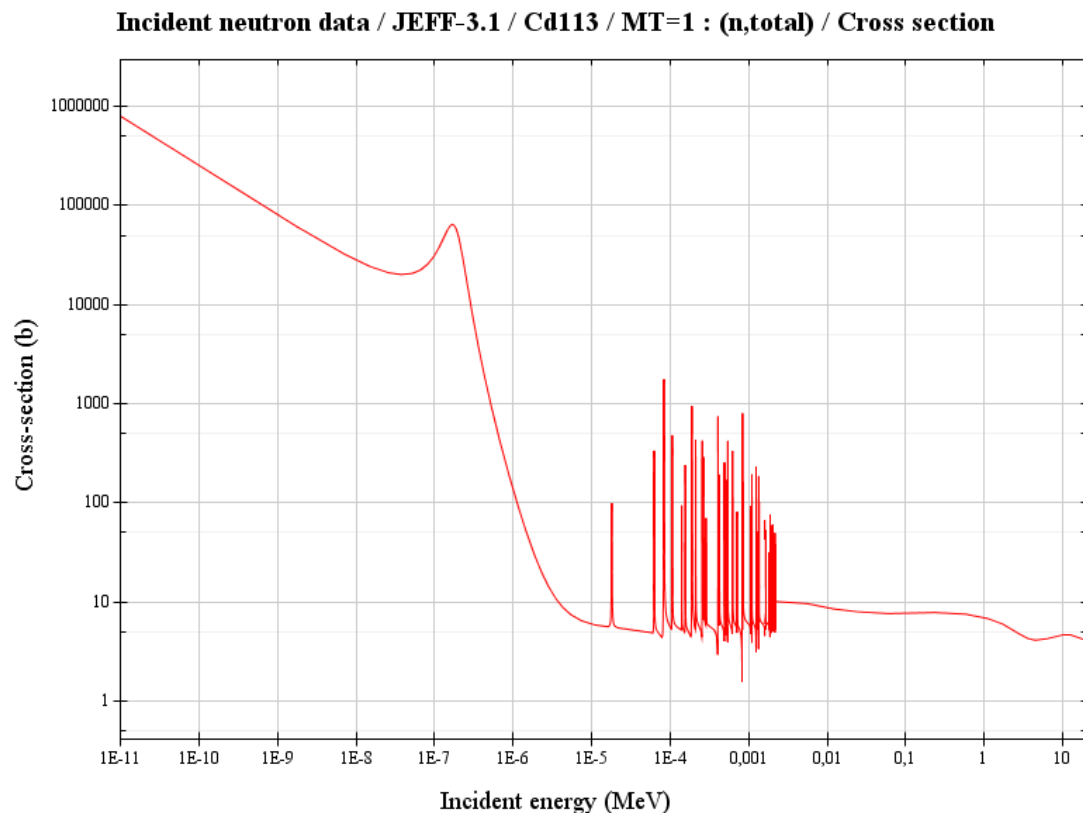


Figure 10. Cadmium 113: total cross-section dependent to the energy. Source: JANIS (Java-based Nuclear Data Information Software); The JEFF-3.1 Nuclear Data Library.

The cadmium is a very good absorber in thermal region since we can note the presence of cadmium cut-off energy for which there is a strong decrease of cross section.

Aluminum and graphite ensure structural integrity to the control rod. They are arranged in such a way to create a bottom plenum and center channel to accommodate air and eventual release of absorption products. Instead, in the upper

part there is a stainless-steel plug to ensure the impermeability. Below, Figure 11 shows three views in different planes of the control rod models.

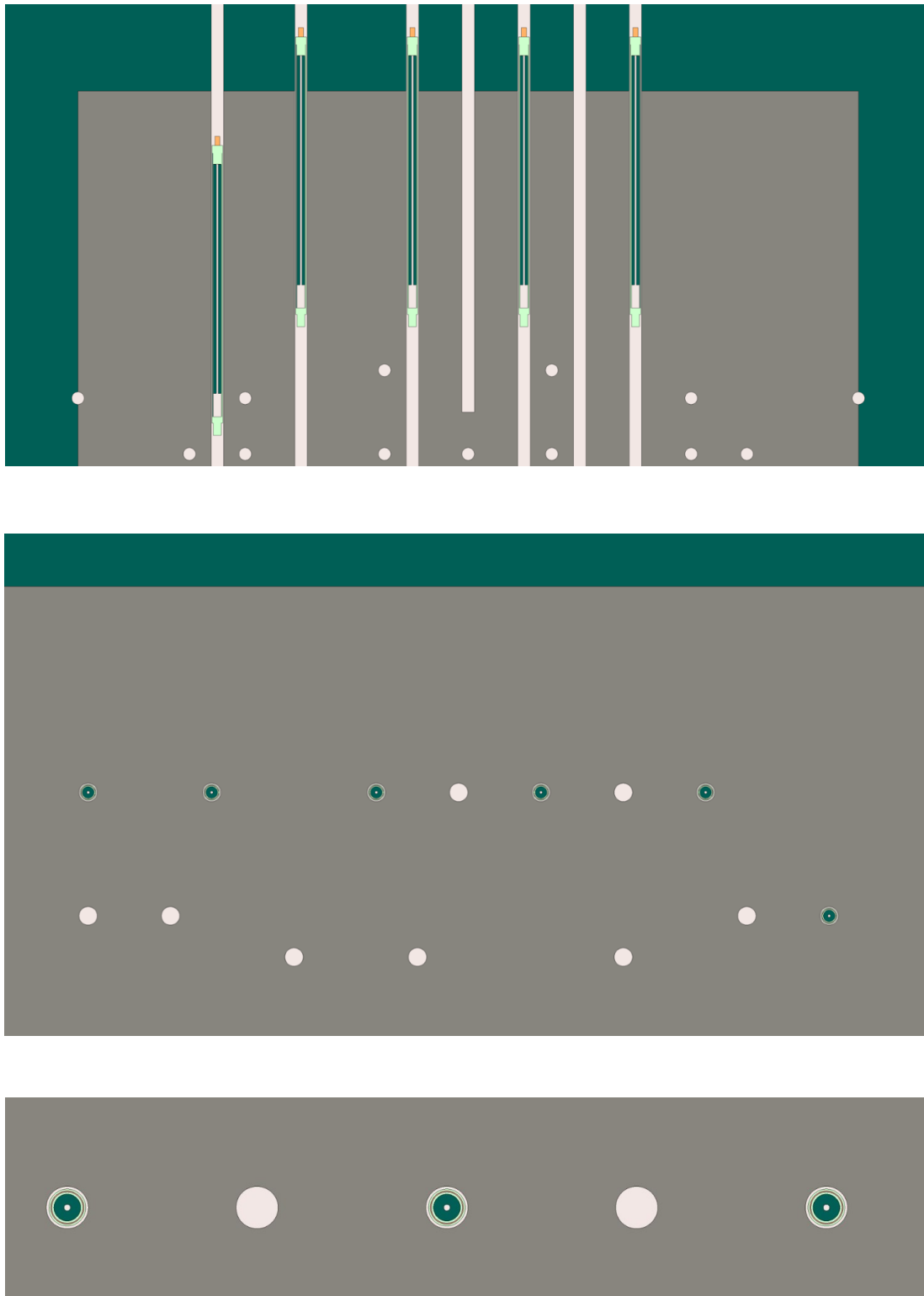


Figure 11. Control rod model. Figure (a) shows the xz plane view with $y = 135$, (b) the xy plane view with $z = 100$ and (c) the zoom on the xy plane view.

In the following table is displayed the isotopic composition and the respectively mass density:

Material	Composition	Approx. density [g/cm3]
Pure Aluminum Alloy	Al-27, Si-28, Fe-56, Cu-63, Cu-65, Mn-55, Mg-24, Mg-25, Mg-26, Zn-64, Ti-46, Ti-47, Ti-48, Ti-49, Ti-50	2.7
Cadmium	Cd-106, Cd-108, Cd-110, Cd-111, Cd-112, Cd-113, Cd-114, Cd-116	8.6
Steel	Fe-54, Fe-56, Fe-57, Fe-58	8.0
Graphite B	C-12, C-13, B-10, B-11	1.6

Table 3. Control rod model isotopic composition.

2.3.4 Biological shielding

Barite concrete serves as the BR1 biological shielding wall. The density is of primary importance to gamma-ray shielding while the neutron attenuation is more dependent upon the presence of light nuclei. The elements that compose the wall ensure a good inelastic and elastic scattering like hydrogen, oxygen and boron but at the same time a good structural stability [26]. The different elements with relative proportion in weight are listed in the following table:

Material	Composition	Approx. density [g/cm3]
Barite concrete	H-1, B-10, B-11, O-16, Mg-24, Mg-25, Mg-26, Al-27, Si-28, Si-29, Si-30, S-32, S-33, S-34, S-36, Ca-40, Ca-42, Ca-43, Ca-44, Ca-46, Ca-48, Fe-54, Fe-56, Fe-57, Fe-58, Ba-130, Ba-132, Ba-134, Ba-135, Ba-136, Ba-137, Ba-138	3.5

Table 4. Barite concrete isotopic composition.

2.4 Source terms

Each transport simulation is performed in criticality steady state condition. The neutron population for the first cycle is defined as source sampled in the fuel material and the number of source neutrons is fixed. The following cycles have as source the neutrons generated by the fission reactions of the previous cycle. The simulation needs a certain number of inactive cycles to allow the initial fission source distribution to converge before starting to collect the results.

2.5 Detectors

In order to compute the neutronics characterization of the BR1, the virtual detectors are introduced in the input file and they must be coupled with the spatial and energy domains. This means that is needed to explain the range of energy and geometries studied. These are used to tally the main results in this study such as neutron spectra, neutron distribution, the power factors in specific channels (Y3, Y4, Y5, Y6 and Y7) and the reaction rates.

Chapter 3

3.1 Simulation and discussion

The simulation is performed with the Serpent code to evaluate the main nuclear indicators that characterize the BR1 core. The robustness of the model is supported by the experimental data, specifications and the MCNP simulation of the reactor.

The code was scheduled to skip 300 inactive cycles to allow the fission source to converge and 1000 active cycles. For each cycle 100 000 neutrons were simulated to have reliable statistics for both core integral parameters such as the effective neutron multiplication factor, as well as local observables such as the neutron flux in a single channel.

3.2 Neutronics parameter

This section summarizes the key integral parameters that describe the neutronic physics of the reactor core calculated with the Serpent model of the BR1 as described in section 2.

3.2.1 Output file

The main core neutronics parameters are calculated by the Serpent code during the transport simulation and are reported as outputs in a Matlab-readable formatted file with extension “_res.m”. Each parameter is identified by an upper-case keyword. For reproducibility purposes we explicitly report in Table 5 the Serpent output keywords used to identify some major neutronics parameters.

Index	Neutronics parameter
IMP_KEFF	Implicit estimate of the k_{eff}
NUBAR	$\bar{\nu}$ (Average number of prompt and delayed neutrons produced per fission)
BETA_EFF	β_{eff} (Effective delayed neutron fraction: total, precursors)
ADJ_NAUCHI_GEN_TIME	Λ_{eff} (Adjoint-weighted neutron generation time using Nauchi's method [27])

Table 5. Some index of Serpent code output file.

The implicit estimate for k_{eff} is calculated as the ratio of the production rate and the loss rate of neutrons:

$$k_{eff,imp} = \frac{\bar{\nu} \cdot R_{fiss}}{R_{fiss} + R_{capture} + R_{Leakage} - R_{inel.scatt}} \quad (3.1)$$

Where R_{fiss} is the total fission rate, $R_{capture}$ is the total capture rate, the $R_{Leakage}$ is the total neutron leakage rate and $R_{inel.scatt}$ is the total inelastic scattering production rate of neutrons from reactions (n,xn) [28].

The BETA_EFF returns the total effective delayed neutron fraction with its uncertainty and the effective delayed neutron fraction of each precursor's group with their uncertainties.

The average number of total neutrons produced per fission $\bar{\nu}$ comes from the index NUBAR and it refers to the average number of neutrons that are released after one fission from prompt and delayed neutron.

3.2.2 Results

The parameters are summarized below:

Core configuration:		
Number of loaded fuel channels	[-]	552
Number of fuel rods per channel	[-]	23
k_{eff}	[pcm]	1.00742 ± 5
$\bar{\nu}$ (Average number of neutrons produced per fission)	[-]	$2.457 \pm 2.7e-6$
Fraction of fissions induced by:		
Thermal energy neutrons (< 0.625 eV)	%	90.02
Intermediate energy neutron (0.625 eV – 100 keV)	%	3.80
Fast energy (> 100 keV)	%	6.18
Point Reactor Kinetics parameters:		
Effective delayed neutron fraction β_{eff}	[pcm]	687 ± 1
Prompt neutron generation time Λ_{eff}	[ms]	1.289 ± 0.0003

Table 6. Neutronics parameters.

The uncertainty of the above parameters are expressed in terms of one standard deviation. This comes only from counting statistics, no other source of uncertainty – e.g. nuclear data, model uncertainties – are included.

The calculated effective neutron multiplication factor k_{eff} is 1.00742 with an error due to counting statistics of 5 pcm.

The average number of neutrons produced per fission $\bar{\nu}$ is equal to 2.457 with an error coming from counting statistics of 1.1×10^{-4} %. This is calculated in the entire core considering any type of fission in any fissionable nuclide and it refers to the total neutrons emitted.

The fraction of neutron-induced fissions is evaluated from the estimate of the fission reaction for three energy regions (thermal below 0.625 eV, intermediate between 0.625 eV and 100 keV and fast above 100 keV). This is calculated as:

$$R_{fiss,therm} \% = \frac{\iiint d^3r \int_0^{E_{thermal}} \sum_j \Sigma_{fiss,j}(r, E) \phi(r, E) dE}{\iiint d^3r \int_0^{\infty} \sum_j \Sigma_{fiss,j}(r, E) \phi(r, E) dE} \cdot 100 \quad (3.2)$$

$$R_{fiss,interm} \% = \frac{\iiint d^3r \int_{E_{thermal}}^{E_{interm}} \sum_j \Sigma_{fiss,j}(r, E) \phi(r, E) dE}{\iiint d^3r \int_0^{\infty} \sum_j \Sigma_{fiss,j}(r, E) \phi(r, E) dE} \cdot 100 \quad (3.3)$$

$$R_{fiss,fast} \% = \frac{\iiint d^3r \int_{E_{interm}}^{E_{fast}} \sum_j \Sigma_{fiss,j}(r, E) \phi(r, E) dE}{\iiint d^3r \int_0^{\infty} \sum_j \Sigma_{fiss,j}(r, E) \phi(r, E) dE} \cdot 100 \quad (3.4)$$

Where j indicates the specific fissionable nuclide and the summation considers all of them, i.e. the atoms of U235 and U238. Moreover the space integration is computed over the entire volume of the core. These results are normalized to the total number of fission reactions in the system.

The effective delayed neutron fraction (β_{eff}) is 687 pcm and the effective prompt neutron generation time (Λ_{eff}) is equal to 1.289 ms. The first parameter accounts the phenomena of the delayed neutrons and the fact that they have different importance inside the reactor. During a fission event, the nucleus involved splits into different fission fragments. Since they are neutron rich atoms in an excited state, some of them can lead by decay to species that can emit neutrons. Such neutrons are called delayed neutrons and the fission fragments that generated them are called precursors of delayed neutrons.

The neutron importance is function of the position \bar{r} with direction $\bar{\Omega}$ and energy E and it is the number of fissions that such neutrons are able to produce [29]. From

reactor kinetics theory is possible to define the delayed neutron fraction weighted by the adjoint neutron flux (ϕ^+) or importance:

$$\beta_{eff} = \frac{\langle \phi^+, F^d \phi \rangle}{\langle \phi^+, F \phi \rangle} \quad (3.5)$$

Where F^d corresponds to the delayed neutron production operator while F is the total prompt and delayed fission neutron production operator and ϕ is the neutron flux [30]. The brackets $\langle \rangle$ define the inner product integrated over all independent variables, i.e. space, energy and angle. This weighting remarks also that the delayed neutrons are emitted with an average energy spectrum of about 150 keV, lower than to the 2 MeV of the prompt neutrons. The value of β_{eff} is a function of the different nuclides and fission rate. In the BR1 the main contribution to the β_{eff} comes from the U235, whose delayed neutron fraction is of 0.65 %.

The Λ_{eff} is the mean generation time between the birth of a fission neutron and the subsequent absorption leading to another fission [31]. It is the timescale of the phenomena that happen in a nuclear reactor. A definition is expressed by the following equation:

$$\Lambda_{eff} = \frac{l_{eff}}{k_{eff}} \quad (3.6)$$

Where l_{eff} is the effective prompt lifetime defined from reactor kinetics as:

$$l_{eff} = \frac{\langle \phi^+, \frac{1}{v} \phi \rangle}{\langle \phi^+, \frac{1}{k_{eff}} F \phi \rangle} \quad (3.7)$$

With v is the neutron speed, ϕ^+ is the adjoint neutron flux, k_{eff} is the effective multiplication factor, ϕ is the neutron flux and F is the total prompt and delayed neutron production operator.

The calculation of these parameters depends on the knowledge of the adjoint flux. Examples of calculations of the adjoint flux using Serpent can be found in the literature [32].

Precursor group, i	$\beta_{eff,i}$ [pcm]	λ_i [1/s]	$T_{\frac{1}{2},i}$ [s]
1	21.91 ± 0.21	0.01335	51.93
2	116.68 ± 0.48	0.03265	21.23
3	114.85 ± 0.49	0.12096	5.73
4	265.68 ± 0.71	0.30472	2.27
5	118.14 ± 0.50	0.85747	0.81
6	49.23 ± 0.31	2.87916	0.24

Table 7. Precursors group data.

In Table 7 there are the point kinetic parameters related to the six-group delayed neutron precursors. The latter are excited fission fragments that emit (delayed) neutrons some appreciable time after the fission as a result of their radioactive decay. Traditionally, the delayed neutrons are represented by six delayed neutron groups of precursors based on half-life.

The number of groups depends on the specific library used since there are six-groups and eight-groups format. For this simulation, the library adopted is ENDF/B-VII,1 that uses the six-groups data.

To obtain the half-life of each group i the following relation is used:

$$T_{\frac{1}{2},i} = \frac{\ln 2}{\lambda_i} \quad (3.8)$$

This represents the amount of time in which half of the original number of radioactive atoms has decayed and it is specific for each isotope.

The main neutronics parameter are compared to the results obtained from the MCNP simulation of the BR1 reactor that is analyzed in the report “*A thorough characterization of the neutron-photon fields in the SCK CEN BR1 research reactor*” [1]. The average number of neutrons produced per fission $\bar{\nu}$ presents a discrepancy of 0.69% less than the one calculated from MCNP, so it is a good agreement. About the fraction of fissions induced by neutrons, in the report the results indicate 90.27% for thermal energy neutrons (< 0.625 eV), 3.64% for intermediate energy neutrons (0.625 eV – 100 keV) and 6.08 % for fast energy neutrons (>100 keV). If we compare the last fraction of fissions induced with the results obtained by Serpent the percentage differences are respectively 0.28%, 4.21% and 1.62%.

From the comparison to the MCNP results, the maximum difference about the effective delayed neutron fraction $\beta_{eff,i}$ is related to the group 6 with an excess discrepancy of 5.24%.

3.3 Power Normalized Factor

The simulation returns qualitative and quantitative values of the neutron indicators that can be normalized to provide a physical dimension. In particular, the power normalization factor (PNF) is introduced to normalize the neutron distribution and the reaction rates.

Notice that output of Serpent is ϕ , i.e. the track length associated to the one source particle in the specific space domain. It is expressed as $\left[\frac{cm}{source}\right]$ but usually we are interested to the flux (density function) so it is necessary to divide the value by the volumetric domain under consideration. In this way we obtain the output ϕ expressed in $\left[\frac{cm}{source\ cm^3}\right]$. As the PNF provides the rates of the particles history $\left[\frac{source}{s}\right]$, we can derive the neutron flux in absolute units:

$$\Phi = \phi \cdot PNF \left[\frac{1}{cm^2\ s}\right] \quad (3.9)$$

Calculation of the PNF requires several input variables:

- Core thermal power in MWth (P)
- Recoverable energy released per fission event in MeV/fission (Q_{fiss})
- The number of fission events per one source particle (n_{fiss})

The thermal power used is the actual power level of the BR1 (0.7 MWth) and the variable Q_{fiss} is assumed to be 200 MeV/fission, the best estimate value for the BR1 core used in the past [1]. The fission energy is partitioned between the fission fragments and the radiation components that include neutrons, gamma rays, beta particles and neutrinos. In a thermal reactor the total energy released for a neutron-induced fission event in U235 is about 210 MeV but not all the total energy can be recovered in a reactor as a fraction is carried out by energetic neutrinos that have a limited probability to interact within the boundaries of the system. The average recoverable energy per fission is lower than the total and it is about 200 MeV per fission.

The number of fission events per one source particle is obtained by the following equation:

$$n_{fiss} = \frac{k_{eff}}{\bar{\nu}} \quad (3.10)$$

The effective neutron multiplication factor k_{eff} and the average number of neutrons produced per fission $\bar{\nu}$ calculated with the Serpent code for the BR1 model are listed in Table 5. These values produce a number of fission events per one source particle equal to 0.41.

The normalization factor can be evaluated with the following equation:

$$PNF = \frac{P}{C n_{fiss} Q_{fiss}} \quad (3.11)$$

Where $C = 1.6022 \times 10^{-13}$ [J/MeV] is a conversion constant to have the energy from Joule to MeV. Applying the above neutronics variables the values of PNF is equal to 5.29×10^{16} [n/s].

3.4 Reaction rates

In this section we estimate reaction rates for the main nuclide presented in the core material: fuel, graphite A, graphite B, cladding and control rods. The mathematical form of the total reaction rate integrated in the specific material volume and over all energy spectra is expressed below:

$$RR_c(\bar{r}) = \int d^3r \int_0^\infty \Sigma_c(\bar{r}, E) \phi(\bar{r}, E) dE \quad (3.12)$$

Where Σ_c is the cross-section for interaction type c and ϕ is the neutron flux evaluated by the transport code. In order to obtain the right physical dimension of the reaction rate we post processing the outcome multiplying by the power normalized factor (PNF). The following tables report the reaction rates divided by nuclides for different materials and by reactions:

Material	Fuel	
Nuclides	U-235	U-238
Fission Rate [1/s]	5.91×10^{19}	2.70×10^{16}
$\Delta_{rel} \%$	0.005	0.022

Capture Rate [1/s]	1.08×10^{19}	4.16×10^{17}
$\Delta_{rel}\%$	0.006	0.006
Elastic Scattering Rate [1/s]	4.42×10^{18}	3.70×10^{18}
$\Delta_{rel}\%$	0.007	0.008
Inelastic Scattering Rate [1/s]	[-]	9.16×10^{16}
$\Delta_{rel}\%$	[-]	0.023

Table 8. Reaction rates of U235 and U238.

Material	Graphite A		
Nuclides	C-Nat	B-10	B-11
Capture Rate [1/s]	4.33×10^{16}	5.60×10^{18}	6.19×10^{16}
$\Delta_{rel}\%$	0.013	0.013	0.013
Elastic Scattering Rate [1/s]	1.19×10^{20}	5.90×10^{19}	1.22×10^{20}
$\Delta_{rel}\%$	0.010	0.010	0.010
Material	Graphite B		
Nuclides	C-Nat	B-10	B-11
Capture Rate [1/s]	1.42×10^{16}	1.84×10^{18}	2.03×10^{16}
$\Delta_{rel}\%$	0.056	0.056	0.056
Elastic Scattering Rate [1/s]	2.69×10^{19}	1.29×10^{19}	2.76×10^{19}
$\Delta_{rel}\%$	0.051	0.051	0.051

Table 9. Reaction rates of graphite A and graphite B.

Material	Cladding	
Nuclides	Al-27	Si-28
Capture Rate [1/s]	5.17×10^{15}	3.74×10^{15}
$\Delta_{rel}\%$	0.045	0.046
Elastic Scattering Rate [1/s]	5.17×10^{15}	3.74×10^{15}
$\Delta_{rel}\%$	0.045	0.046

Table 10. Reaction rates of cladding.

Material	Control rod		
Nuclides	Al	Stainless Steel	Cd
Capture Rate [1/s]	8.64×10^{12}	1.22×10^{12}	3.75×10^{14}
$\Delta_{rel}\%$	0.35	1.76	0.13

Table 11. Reaction rates of control rod.

All result estimates are accompanied by the associated relative statistical errors in percentage, $\Delta_{rel,\%}$.

Although U238 has a much lower capability to achieve fissions than U235 due to a lower microscopic cross section, its high quantity in the reactor implies that the fission reaction rate of U238 is not negligible.

We note the high rate of elastic scattering reaction by graphite A and graphite B, which is also the result of the low atomic number of the nuclides of which they are composed. This demonstrates a good neutron slowing capacity in order to obtain the thermal neutron spectrum of the reactor.

The cladding material also contributes to both capture and neutron elastic scattering phenomena. It is noted that the order of magnitude of the reaction rates are lower as we have both a smaller amount of this material and nuclides that have less capability to interact with neutrons.

Finally, the capture rates of the control rods relative to the main nuclides present are reported. These reaction rates are relative to a control rod configuration in the steady state operating of the reactor.

3.5 Neutron spectra

The neutron spectra are evaluated for the empty channels parallel to the x axis that can accommodate instrumentations: Y3, Y4, Y5, Y6 and Y7. The characterization is performed over the whole energy domains of the neutron flux considering a discretization of 725 energy bins uniformly spaced. It is necessary to remark that the Serpent code does not calculate the point value of the neutron flux on the energy but it computes an integral evaluation on a specific energy interval.

We divided the energy-integrated neutron spectra by the bin to remove the dependence on the energy binning, hence allowing further comparison with spectra calculated using a different grid. In other words, the energy integrated neutron spectra become the average value inside of each energy bin. Below, there is the mathematical form:

$$\bar{\varphi}_i = \frac{\int_{E_{i-1}}^{E_i} \varphi_i(E) dE}{\Delta E_i} \quad (3.13)$$

Where $\int_{E_{i-1}}^{E_i} \varphi_i(E) dE$ is the energy integrated neutron spectra over the energy bin i and $\bar{\varphi}_i$ is the averaged neutron spectra associated to the energy bin i . The ΔE_i is the difference between the upper and lower boundaries of the bin i as following:

$$\Delta E_i = E_i - E_{i-1} \quad (3.14)$$

The normalization was done in such a way to ensure the following equation:

$$\begin{aligned} \int_0^{\infty} \varphi(E) dE &= \int_{E_0}^{E_1} \varphi_1(E) dE + \int_{E_1}^{E_2} \varphi_2(E) dE + \dots + \int_{E_{N-1}}^{E_N} \varphi_N(E) dE \\ &\cong \sum_{i=1}^N \bar{\varphi}_i \Delta E_i = 1 \end{aligned} \quad (3.15)$$

With N is the number of total energy bins and i is the number of specific energy bin. At this point we divided the averaged neutron spectra of each bin by the total integrated neutron spectra calculated as Eq.(3.16). The normalization is:

$$\check{\varphi}_i = \frac{\bar{\varphi}_i}{\sum_{i=1}^N \bar{\varphi}_i \Delta E_i} = \frac{\bar{\varphi}_i}{\varphi_{tot}} \quad (3.16)$$

Where φ_{tot} is the total integrated neutron spectra and $\check{\varphi}_i$ is the normalized neutron spectra of bin i . The latter is adimensional unit energy integrated neutron flux and it is represented in Figure 12.

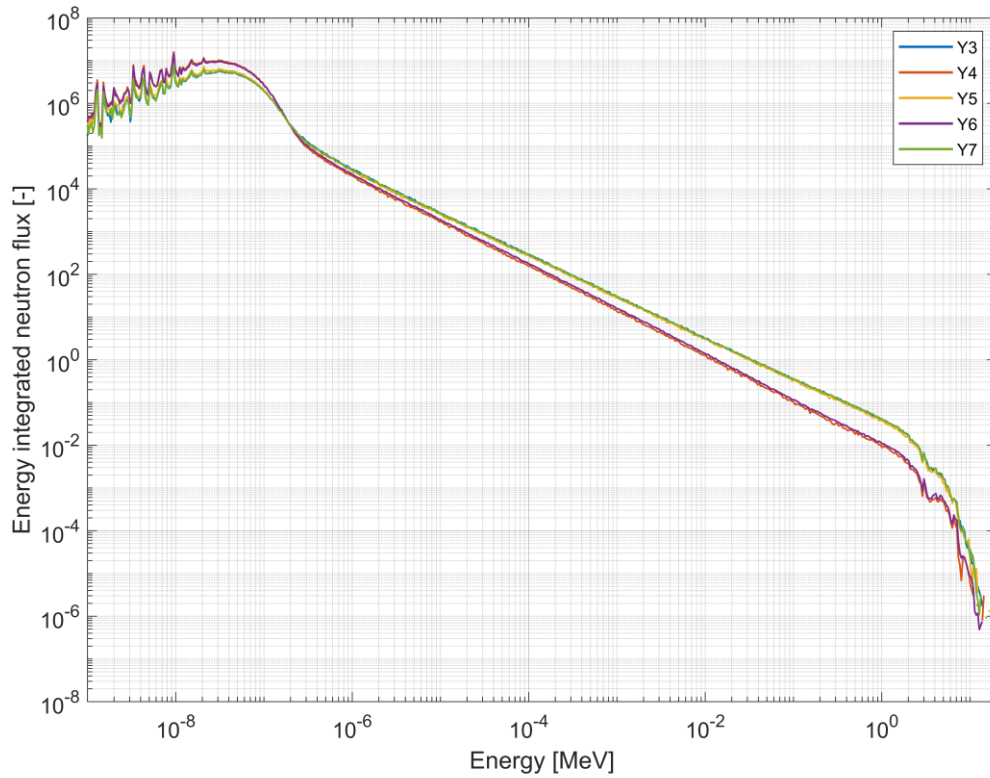


Figure 12. Neutron Spectra for channels Y3, Y4, Y5, Y6 and Y7.

The enhanced flux in the thermal region in all analyzed channels is a consequence of the graphite moderator that slows down the neutrons and increases the probability to have fission reaction. The linear behavior in the intermediate energy region is typical of a $1/E$ dependency. This dependence is caused by the nature of the slowing down process due to scattering process. Figure 13 shows the elastic scattering cross of natural carbon that presents almost constant value at intermediate energy.

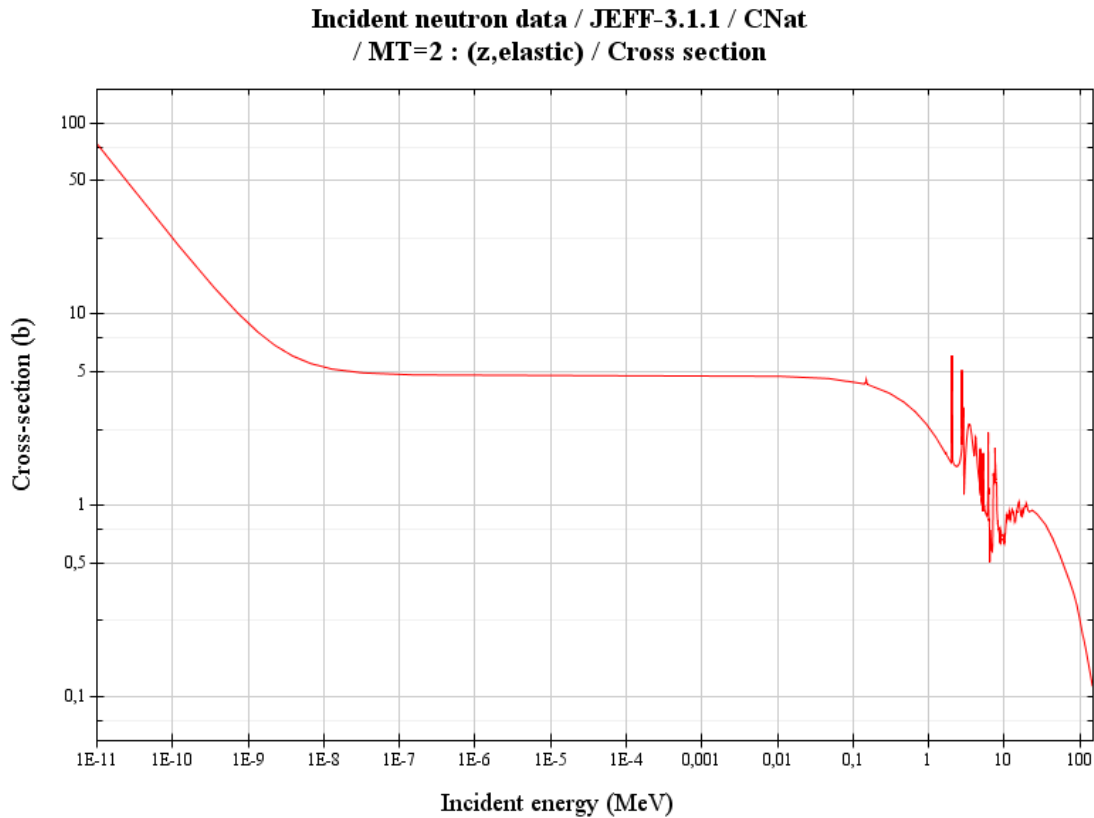


Figure 13. Elastic cross section of carbon-12. Source: JANIS (Java-based Nuclear Data Information Software); The JEFF-3.1.1 Nuclear Data Library.

Table 12 shows the energy integrated neutron flux of channels Y3, Y4, Y5, Y6 and Y7. In absolute terms the channels Y4 and Y6 present the integrated neutron flux higher than the other channels. There are two reasons that could justify this behavior and both of them are related to the lack of fuel around the channels Y4 and Y6. The first reason depends on the less capture rate of the thermal neutrons due to the presence of parasitic capture in the fuel. The second one is related to the higher probability that distant fast neutrons could thermalize as they have more space to do it. Moreover, there are very fewer fast neutrons since it does not occur fissions in the near channels. In absolute terms for channels Y4 and Y6 there is also an integrated neutron flux in the fast spectrum lower than the others.

The neutron flux for channels Y3, Y5 and Y7 is very similar between them since they are located quite symmetrically in the core geometry. Below,

Figure 14 displays the energy integrated neutron flux divided in three regions, in particular a thermal region ($E < 0.55$ eV), an intermediate region ($0.55 \text{ eV} < E < 100 \text{ keV}$) and a fast spectrum region ($E > 100 \text{ keV}$).

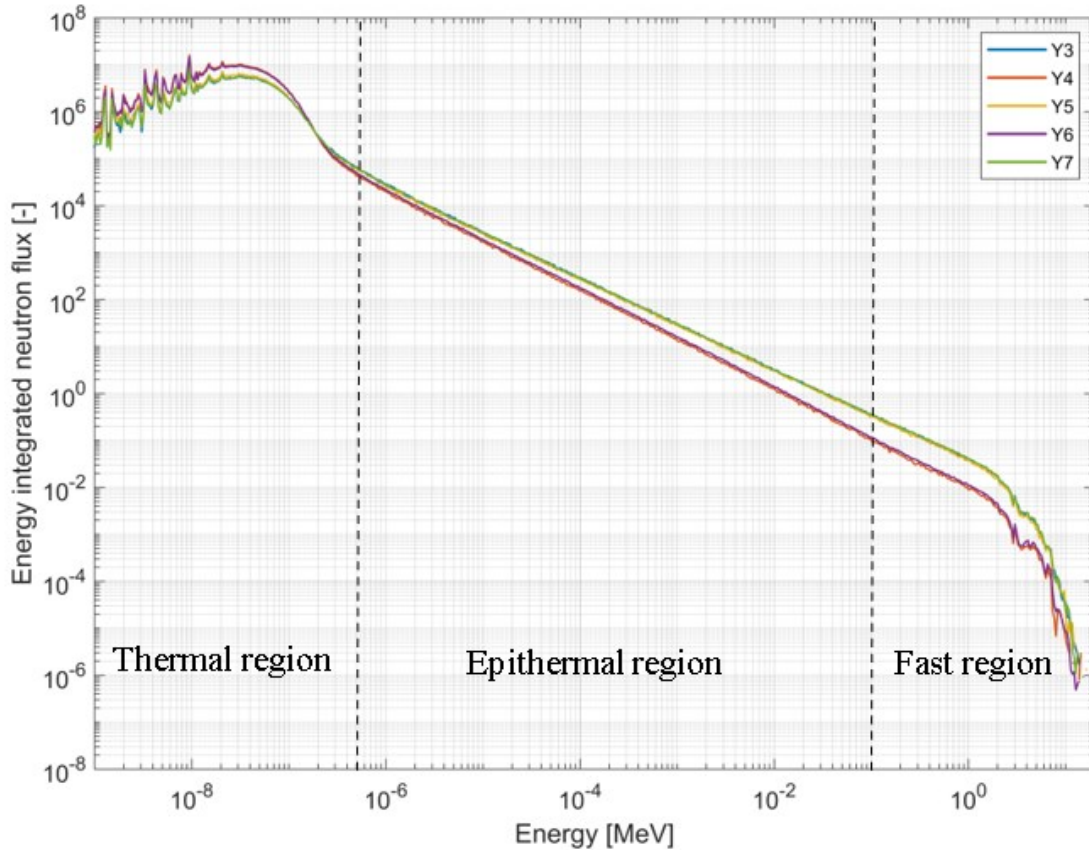


Figure 14. Neutron Spectra with energy subdivisions.

Below we can find in Table 12 that summarize the total flux for each different channel and the total flux inside a 20-cm long segment in the middle of the x axis of each channel.

Channel	Total Flux [1/(cm ² s)]	Total Flux in the segment [1/(cm ² s)]
Y3	3.38x10 ¹¹	5.24x10 ¹¹
Y4	3.71x10 ¹¹	5.76x10 ¹¹
Y5	3.71x10 ¹¹	5.79x10 ¹¹
Y6	3.40x10 ¹¹	5.27x10 ¹¹
Y7	2.90x10 ¹¹	4.54x10 ¹¹

Table 12. Total neutron flux for each channel.

These values are normalized by the power normalized factor (PNF) defined in the previous section. We can note that the total neutron flux in the segment is higher than the entire channel ones. This is due to the fact that the detection of the neutron flux in the cell is in the middle of the channel, that is in the point in which the value of the flux is the highest along the x-axis.

3.6 Neutron flux distribution

The neutron flux distribution is computed for the channel Y3, Y4, Y5, Y6 and Y7. This represents the neutron flux along the x axis, from $x = 330$ cm to $x = -330$ cm. For each channel the thermal flux, the epithermal and fast flux and the total neutron flux were evaluated. The threshold between the thermal and epithermal/fast region is assumed 0.55 eV according to the previous assumption. The detector used to evaluate the flux is considered for entire volume channel. Below, we can find the plots that visualize the distribution flux for each channel:

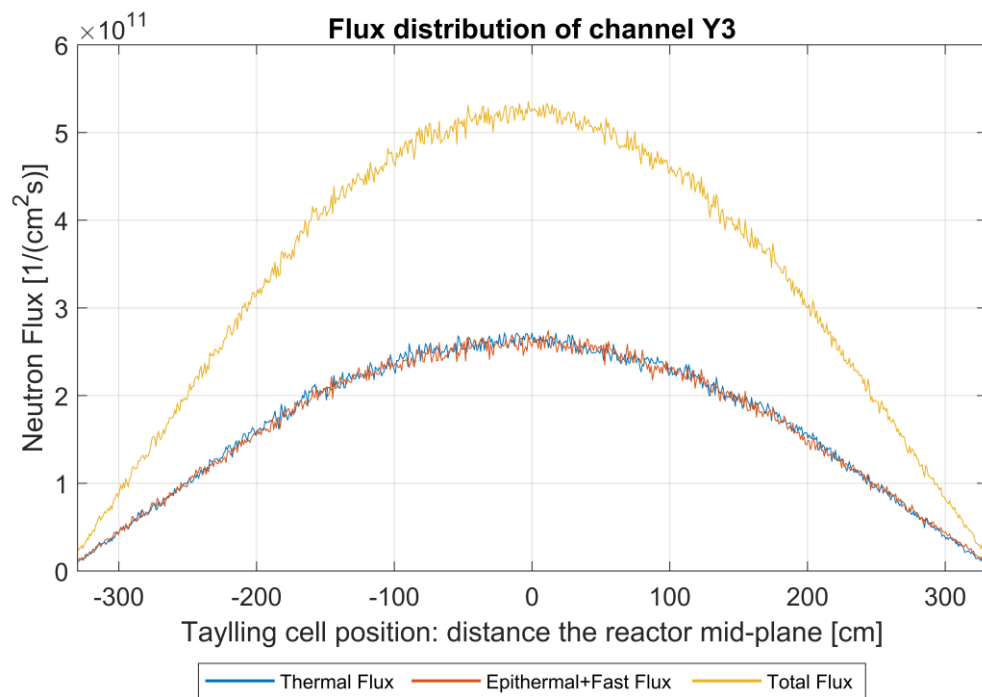


Figure 15. Neutron flux distribution of channel Y3.

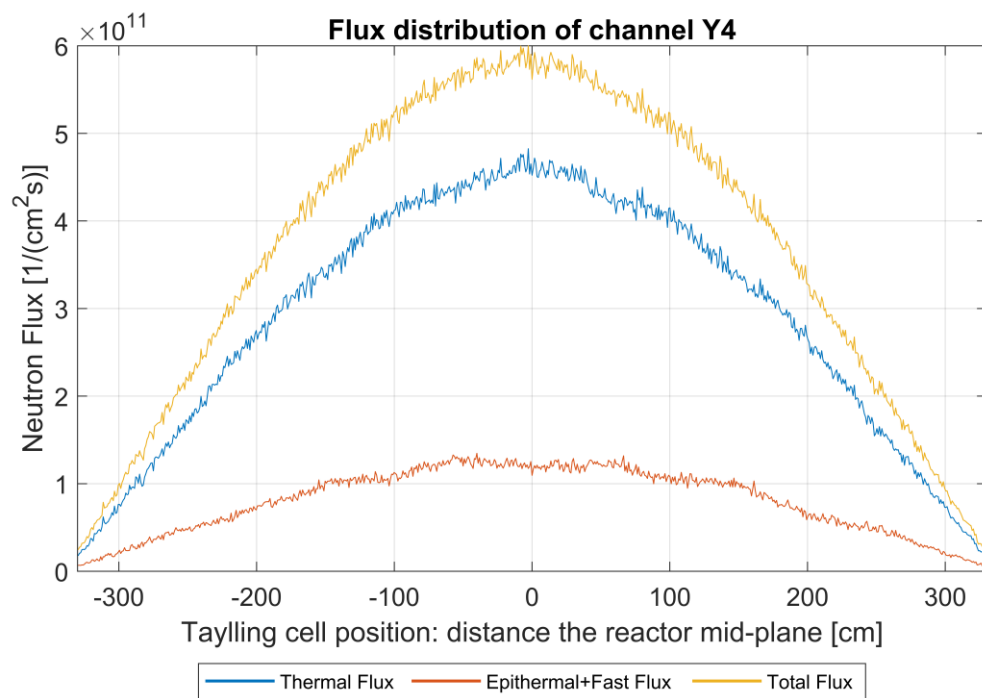


Figure 16. Neutron flux distribution of channel Y4

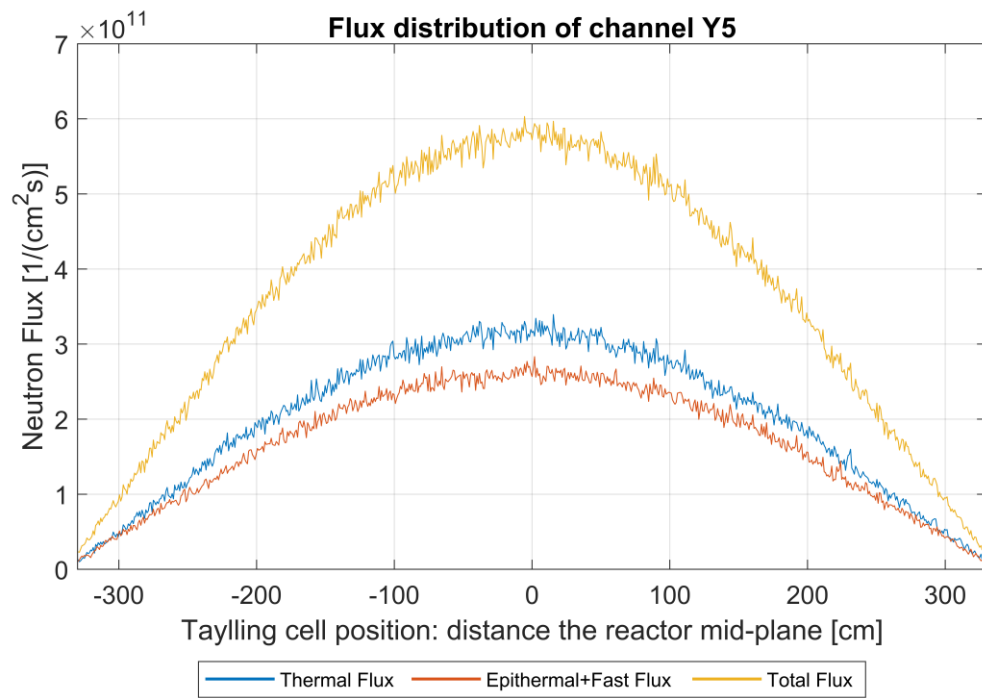


Figure 17. Neutron flux distribution of channel Y5.

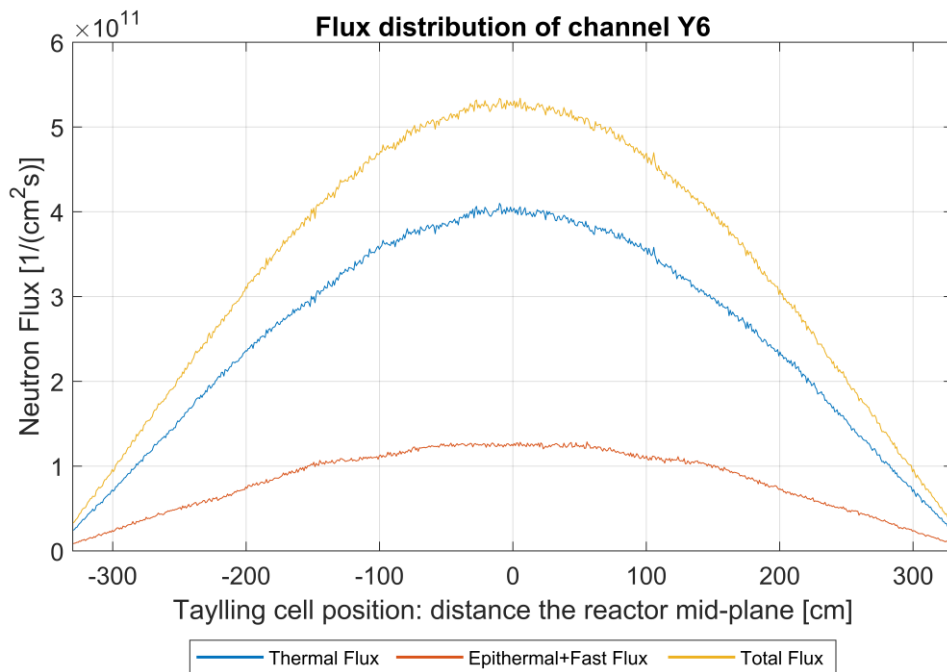


Figure 18. Neutron flux distribution of channel Y6.

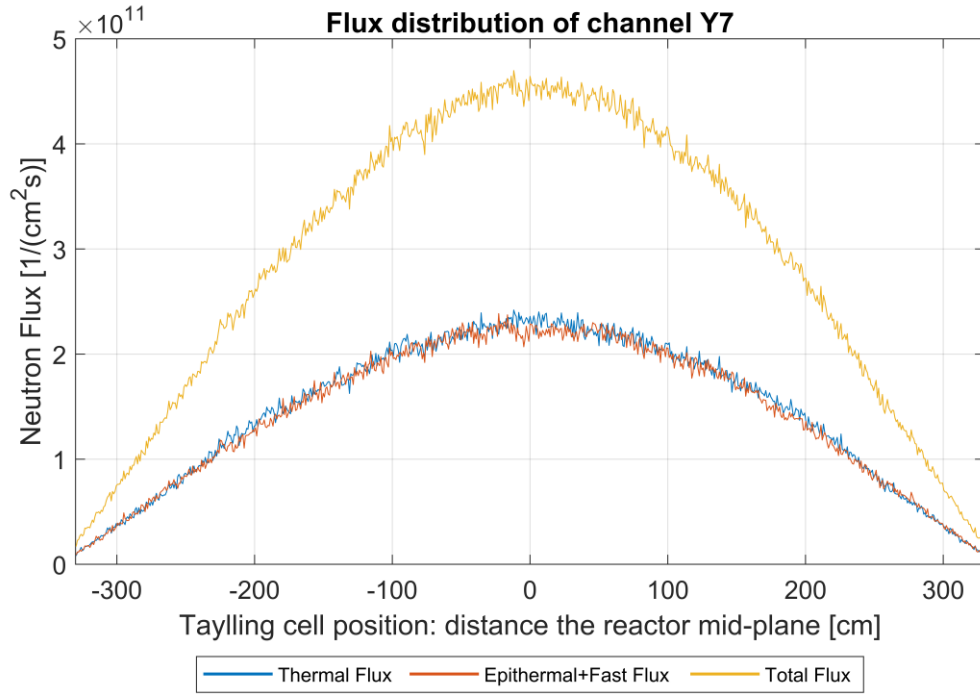


Figure 19. Neutron flux distribution of channel Y7.

Also in this case the evolution of the different flux can be grouped. The channels Y4 and Y6 have a similar behavior: the thermal flux is higher than the one related to the intermediate and fast energy region. Moreover, the Y6 channel has the flux one order of magnitude higher than the other channels.

The channels Y3, Y5 and Y7 have the thermal and epithermal/fast neutron flux very similar. We can observe that the flux is symmetric respect to the center of the channel, at $x = 0$.

3.7 Power map

A power map over all channels with fuel can be described by power factors (PF). These are defined as the ratio between the power of each channel with fuel to the average power of the core:

$$PF_i = \frac{P_{channel,i}}{P_{avg,core}} \quad (3.17)$$

Where the power $P_{channel,i}$ is evaluated starting from the fission rate and the neutron flux inside of fuel:

$$P_{channel,i} = Q_{fiss} \cdot \iiint d^3r \int_0^\infty \Sigma_{fission,i}(r,E) \phi_i(r,E) dE \quad (3.18)$$

Where the $\Sigma_{fission,i}(r,E)$ and $\phi_i(r,E)$ are respectively the macroscopic fission cross section and the neutron flux related to the specific channel i .

The average core power is calculated as the sum of all power channels divided by the number of channels with the fuel:

$$P_{avg,core} = \frac{\sum_i^{N_{channel}} P_{channel,i}}{N_{channel}} \quad (3.19)$$

$N_{channel}$ is the number of channels that contain the fuel, i.e. 552.

According to the definition of the power factors we can demonstrate that the sum of all of them returns the total number of channels filled with nuclear fuel.

Hence, the power distribution in the BR1 core defined in terms of power factors is displayed in Figure 20. The peak factor is located between the Y4 and Y6 channels and the value is 1.87 in the yellow cell while the minimum factor is 0.30 in the blue cell.

	12	11	10	9	8	7	6	5	4	3	2	1	0	-1	-2	-3	-4	-5	-6	-7	-8	-9	-10	-11	-12	-13
13								0.58	0.59	0.63	0.65	0.67	0.67	0.66	0.64	0.60	0.55	0.52								
12	POWER FACTORS							0.67	0.69	0.72	0.75	0.77	0.77	0.75	0.73	0.69	0.64	0.58	0.54	0.49						
11								0.77	0.79	0.83	0.87	0.90	0.92	0.91	0.89	0.87	0.82	0.76	0.68	0.61	0.53	0.47	0.41			
10					0.73	0.79	0.84	0.91	0.97	1.01	1.04	1.07	1.06	1.04	1.00	0.95	0.88	0.80	0.70	0.60	0.51	0.45				
9				0.72	0.78	0.87	0.97	1.05	1.11	1.14	1.18	1.20	1.19	1.16	1.13	1.06	0.99	0.89	0.78	0.66	0.56	0.48	0.42			
8			0.70	0.77	0.88	0.99	1.09	1.17	1.22	1.26	1.28	1.30	1.29	1.27	1.23	1.17	1.08	0.97	0.81	0.68	0.58	0.49	0.41	0.36		
7		0.65	0.73	0.85	0.98	1.10	1.19	1.27	1.33	1.35	1.35	1.36	1.38	1.37	1.33	1.26	1.18	1.06	0.90	0.77	0.66	0.56	0.46	0.39	0.34	
6		0.71	0.80	0.94	1.08	1.20	1.29	1.37	1.42	1.44	1.43	1.44	1.47	1.46	1.42	1.36	1.28	1.17	1.05	0.92	0.80	0.68	0.56	0.47	0.40	
5		0.76	0.87	1.02	1.15	1.27	1.37	1.44	1.49	1.51	1.52	1.55	1.54	1.52	1.49	1.44	1.36	1.26	1.14	1.01	0.90	0.78	0.65	0.55	0.45	0.39
4	0.70	0.79	0.93	1.08	1.22	1.33	1.43	1.49	1.54	1.56	1.59	1.61	1.59	1.57	1.54	1.49	1.42	1.33	1.22	1.10	0.98	0.86	0.73	0.61	0.51	0.43
3	0.70	0.82	0.97	1.12	1.26	1.37	1.47	1.53	1.59	1.65	1.76	1.78	1.67	1.61	1.58	1.54	1.48	1.39	1.29	1.18	1.06	0.93	0.80	0.68	0.56	0.48
2	0.73	0.84	1.00	1.15	1.29	1.41	1.49	1.56	1.64	1.85			1.86	1.67	1.63	1.63	1.54	1.44	1.34	1.23	1.11	0.98	0.85	0.72	0.59	0.51
1	0.75	0.86	1.02	1.17	1.31	1.42	1.50	1.56	1.70					1.71	1.67		1.61	1.46	1.36	1.25	1.13	1.00	0.86	0.74	0.61	0.53
0	0.75	0.86	1.02	1.17	1.30	1.40	1.49	1.54	1.62	1.82			1.83	1.63	1.59	1.62	1.53	1.44	1.35	1.24	1.13	1.00	0.86	0.74	0.61	0.53
-1	0.74	0.84	1.00	1.16	1.29	1.39	1.47	1.51	1.56	1.66	1.82	1.87	1.74	1.60	1.55	1.53	1.48	1.41	1.32	1.22	1.10	0.98	0.86	0.72	0.60	0.52
-2	0.71	0.82	0.98	1.13	1.26	1.36	1.44	1.49	1.53	1.67				1.66	1.52	1.48	1.43	1.36	1.28	1.18	1.07	0.95	0.83	0.70	0.58	0.49
-3	0.68	0.79	0.94	1.08	1.21	1.32	1.40	1.45	1.50	1.66				1.64	1.47	1.41	1.37	1.30	1.20	1.10	0.99	0.88	0.77	0.65	0.53	0.46
-4	0.67	0.75	0.89	1.03	1.15	1.26	1.34	1.39	1.43	1.56				1.54	1.40	1.35	1.28	1.21	1.10	1.00	0.90	0.79	0.68	0.57	0.47	0.40
-5		0.72	0.82	0.95	1.08	1.18	1.26	1.32	1.36	1.40	1.49	1.53	1.48	1.39	1.32	1.26	1.20	1.11	1.01	0.91	0.80	0.70	0.60	0.50	0.41	0.36
-6		0.67	0.75	0.87	0.99	1.10	1.18	1.23	1.27	1.28	1.26	1.27	1.29	1.26	1.22	1.17	1.10	1.01	0.90	0.79	0.69	0.60	0.50	0.42	0.37	
-7		0.61	0.67	0.78	0.89	0.99	1.07	1.13	1.17	1.18	1.16	1.17	1.17	1.15	1.10	1.04	0.97	0.87	0.74	0.64	0.55	0.47	0.39	0.34		
-8			0.63	0.69	0.79	0.88	0.96	1.02	1.06	1.08	1.09	1.09	1.08	1.06	1.01	0.94	0.87	0.78	0.65	0.55	0.47	0.39	0.33	0.30		
-9				0.64	0.69	0.76	0.84	0.90	0.94	0.97	0.99	1.00	0.98	0.96	0.92	0.86	0.80	0.71	0.62	0.53	0.45	0.38	0.34			
-10					0.64	0.68	0.73	0.78	0.82	0.85	0.86	0.88	0.86	0.84	0.80	0.76	0.69	0.63	0.56	0.47	0.41	0.35				
-11								0.66	0.69	0.72	0.74	0.75	0.73	0.71	0.69	0.65	0.59	0.54	0.48	0.42	0.37	0.33				
-12								0.57	0.59	0.63	0.65	0.65	0.63	0.62	0.61	0.57	0.53	0.48	0.42	0.38						
-13								0.49					0.58													

Figure 20. Power map of BR1.

The power factors higher than the unity have a power channel greater than the average power. The maximum power generation is in the centre of the core and the values under the unity are located mainly in the periphery.

For each power factor channel it is calculated the relative statistical error expressed in percentage. The map below shows that the peak factor has a relative error of 0.20% and for the minimum power factor the relative error is 0.53%.

The power map represented in Figure 20 was also calculated with the MCNP code [33]. The peak power factor for the hot channel in that case was 1.82 while the minimum value was 0.274, in similar locations to our case. The respectively discrepancies in percentage between the values obtain with Serpent are 2.67% and 8.67%.

	12	11	10	9	8	7	6	5	4	3	2	1	0	-1	-2	-3	-4	-5	-6	-7	-8	-9	-10	-11	-12	-13
13								0.38	0.35	0.35	0.34	0.34	0.34	0.34	0.35	0.37	0.38	0.38								
12	RELATIVE ERROR [%]							0.33	0.34	0.32	0.32	0.30	0.32	0.31	0.33	0.33	0.35	0.36	0.39	0.40						
11							0.32	0.30	0.31	0.30	0.29	0.29	0.29	0.30	0.30	0.31	0.32	0.34	0.38	0.38	0.40	0.44				
10					0.33	0.31	0.29	0.29	0.28	0.28	0.27	0.27	0.26	0.27	0.28	0.29	0.29	0.31	0.33	0.36	0.39	0.41				
9				0.33	0.31	0.30	0.28	0.26	0.26	0.26	0.25	0.25	0.25	0.24	0.24	0.24	0.26	0.25	0.26	0.28	0.30	0.33	0.36	0.38	0.43	0.45
8			0.34	0.33	0.30	0.28	0.26	0.26	0.25	0.25	0.24	0.24	0.24	0.24	0.26	0.25	0.26	0.28	0.30	0.33	0.36	0.38	0.43	0.45		
7		0.35	0.33	0.30	0.28	0.26	0.25	0.24	0.23	0.23	0.23	0.23	0.23	0.24	0.24	0.24	0.25	0.26	0.27	0.32	0.35	0.36	0.37	0.44	0.45	
6		0.34	0.31	0.28	0.27	0.25	0.25	0.24	0.23	0.23	0.21	0.22	0.23	0.22	0.23	0.24	0.24	0.25	0.27	0.29	0.30	0.32	0.37	0.39	0.44	
5		0.31	0.29	0.28	0.26	0.25	0.24	0.23	0.22	0.21	0.23	0.21	0.23	0.22	0.22	0.23	0.22	0.24	0.25	0.26	0.29	0.31	0.33	0.37	0.42	0.45
4	0.33	0.29	0.29	0.27	0.26	0.24	0.24	0.23	0.22	0.23	0.21	0.21	0.22	0.22	0.22	0.22	0.23	0.24	0.24	0.26	0.28	0.30	0.31	0.35	0.38	0.42
3	0.33	0.30	0.29	0.26	0.24	0.23	0.23	0.22	0.21	0.22	0.20	0.20	0.21	0.20	0.21	0.22	0.22	0.24	0.24	0.25	0.27	0.28	0.31	0.32	0.35	0.40
2	0.32	0.31	0.26	0.25	0.24	0.23	0.23	0.21	0.22	0.20			0.20	0.21	0.21	0.21	0.22	0.23	0.23	0.25	0.26	0.27	0.29	0.33	0.35	0.37
1	0.31	0.29	0.28	0.25	0.23	0.24	0.23	0.22	0.22					0.20	0.20		0.22	0.22	0.23	0.24	0.26	0.28	0.29	0.33	0.35	0.38
0	0.32	0.30	0.27	0.24	0.24	0.23	0.24	0.21	0.21	0.20			0.20	0.21	0.22	0.21	0.21	0.23	0.23	0.25	0.24	0.28	0.30	0.32	0.34	0.40
-1	0.33	0.30	0.27	0.25	0.24	0.23	0.23	0.22	0.21	0.21	0.20	0.20	0.21	0.21	0.22	0.22	0.22	0.22	0.23	0.24	0.25	0.29	0.30	0.31	0.36	0.41
-2	0.34	0.30	0.30	0.25	0.25	0.24	0.23	0.22	0.22	0.21				0.21	0.21	0.22	0.22	0.23	0.24	0.25	0.27	0.28	0.31	0.34	0.35	0.40
-3	0.33	0.32	0.28	0.27	0.25	0.24	0.24	0.23	0.23	0.22				0.21	0.22	0.23	0.24	0.23	0.25	0.26	0.28	0.30	0.31	0.36	0.37	0.41
-4	0.35	0.34	0.30	0.28	0.27	0.26	0.23	0.23	0.22	0.22				0.22	0.23	0.23	0.25	0.24	0.27	0.28	0.28	0.32	0.33	0.37	0.38	0.43
-5		0.32	0.30	0.28	0.27	0.26	0.25	0.24	0.23	0.23	0.22	0.22	0.22	0.22	0.24	0.25	0.25	0.27	0.28	0.28	0.31	0.32	0.35	0.38	0.42	0.45
-6		0.35	0.33	0.30	0.28	0.26	0.25	0.25	0.25	0.24	0.24	0.23	0.23	0.23	0.24	0.26	0.25	0.27	0.29	0.31	0.33	0.35	0.38	0.44	0.45	
-7		0.37	0.34	0.32	0.29	0.27	0.26	0.27	0.26	0.24	0.25	0.26	0.25	0.25	0.25	0.26	0.26	0.28	0.30	0.34	0.36	0.40	0.43	0.46		
-8			0.34	0.33	0.32	0.30	0.29	0.27	0.26	0.26	0.25	0.25	0.25	0.26	0.28	0.27	0.30	0.31	0.33	0.36	0.41	0.44	0.48	0.53		
-9				0.34	0.33	0.32	0.31	0.28	0.28	0.28	0.27	0.28	0.27	0.28	0.28	0.29	0.31	0.35	0.36	0.39	0.41	0.45	0.49			
-10					0.35	0.33	0.32	0.32	0.30	0.30	0.29	0.28	0.29	0.29	0.32	0.30	0.33	0.34	0.36	0.40	0.41	0.48				
-11						0.36	0.34	0.34	0.32	0.31	0.32	0.31	0.32	0.33	0.35	0.35	0.35	0.39	0.42	0.43	0.45	0.47				
-12							0.37	0.36	0.36	0.35	0.33	0.35	0.34	0.36	0.36	0.36	0.38	0.39	0.42	0.44						
-13							0.40						0.36													

Figure 21. Relative error of the power factors.

3.8 Sensitivity analysis

The sensitivity analysis is used to assess how the results change when we change our model's assumptions. This is an essential part of the evaluation on the robustness and validity of our outcomes.

3.8.1 Impact of different library

In this section the main objective is to evaluate the impact of the different library on the main neutronics results and compare them with the Serpent simulation outcomes obtained before.

All the results up to now were simulated using the ENDF/B-VII.1 library. We perform again the power factors, the power normalized factor (PNF) and the main neutronics parameters changing the other available libraries in the cluster: JEFF-3.1.2, JEFF-3.3, JENDL-4.0u and ENDF/B-VIII.0. For each of them all the assumptions explained before are valid.

For each case, a table is built that summarizes the main parameters and percentage discrepancies with respect to the ENDF/B-VII.1 library. Moreover, two maps are displayed to visualize the power factors and relative statistical errors.

3.8.1.1 Simulation with JEFF-3.1.2

Neutronics parameter			with JEFF – 3.2.1	with ENDF/B - VII.1	Discrepancies
Effective multiplication factor	k_{eff}	[-]	1.01799 ± 0.00005	1.00742 ± 0.00005	1.04 %
Effective delayed neutron fraction	β_{eff}	[pcm]	707 ± 1	687 ± 1	2.83 %
Prompt neutron generation time	Λ_{eff}	[ms]	1.302 ± 0.0004	1.289 ± 0.0003	0.99 %
Power Normalized Factor	PNF	[n/s]	5.18×10^{16}	5.29×10^{16}	-2.12 %

Table 13. Neutronics parameter with JEFF 3.2.1 library.

	12	11	10	9	8	7	6	5	4	3	2	1	0	-1	-2	-3	-4	-5	-6	-7	-8	-9	-10	-11	-12	-13
13								0.59	0.60	0.64	0.66	0.68	0.68	0.66	0.64	0.60	0.56	0.53								
12	POWER FACTORS, JEFF 3.2.1							0.68	0.70	0.73	0.75	0.77	0.77	0.76	0.73	0.69	0.64	0.59	0.54	0.49						
11							0.78	0.79	0.83	0.87	0.89	0.92	0.91	0.90	0.86	0.81	0.75	0.69	0.61	0.53	0.47	0.41				
10					0.74	0.80	0.85	0.92	0.97	1.01	1.05	1.06	1.05	1.03	1.00	0.94	0.87	0.79	0.69	0.60	0.51	0.45				
9				0.73	0.79	0.88	0.97	1.05	1.11	1.14	1.17	1.20	1.18	1.15	1.12	1.05	0.98	0.88	0.77	0.65	0.56	0.47	0.42			
8			0.71	0.78	0.88	0.99	1.09	1.17	1.22	1.25	1.27	1.30	1.29	1.26	1.22	1.15	1.07	0.96	0.80	0.68	0.57	0.48	0.40	0.36		
7		0.67	0.73	0.86	0.98	1.10	1.20	1.27	1.32	1.34	1.34	1.36	1.38	1.36	1.32	1.25	1.16	1.04	0.89	0.76	0.65	0.55	0.46	0.38	0.34	
6		0.72	0.81	0.94	1.08	1.19	1.30	1.37	1.42	1.44	1.42	1.44	1.47	1.45	1.42	1.34	1.27	1.16	1.03	0.91	0.79	0.67	0.55	0.46	0.40	
5		0.77	0.88	1.02	1.16	1.27	1.37	1.45	1.49	1.51	1.53	1.54	1.54	1.52	1.49	1.43	1.35	1.25	1.12	1.00	0.88	0.76	0.65	0.54	0.45	0.39
4	0.71	0.80	0.94	1.09	1.22	1.33	1.43	1.50	1.54	1.57	1.60	1.61	1.59	1.56	1.54	1.48	1.41	1.31	1.20	1.08	0.96	0.84	0.72	0.61	0.50	0.43
3	0.72	0.82	0.97	1.14	1.27	1.38	1.48	1.53	1.60	1.67	1.78	1.80	1.68	1.61	1.58	1.54	1.47	1.37	1.27	1.16	1.04	0.92	0.80	0.67	0.55	0.48
2	0.74	0.85	1.01	1.17	1.29	1.41	1.50	1.57	1.66	1.88			1.87	1.68	1.63	1.63	1.54	1.42	1.32	1.21	1.10	0.97	0.84	0.71	0.59	0.51
1	0.76	0.86	1.02	1.17	1.31	1.43	1.51	1.57	1.72					1.72	1.67		1.59	1.45	1.34	1.24	1.12	0.99	0.84	0.72	0.61	0.53
0	0.76	0.86	1.02	1.16	1.30	1.41	1.49	1.55	1.64	1.85			1.85	1.63	1.60	1.61	1.52	1.43	1.33	1.22	1.11	0.99	0.85	0.73	0.61	0.54
-1	0.74	0.85	1.01	1.14	1.28	1.39	1.48	1.52	1.57	1.68	1.86	1.90	1.76	1.62	1.56	1.52	1.47	1.40	1.31	1.20	1.09	0.97	0.84	0.72	0.60	0.52
-2	0.72	0.83	0.98	1.13	1.26	1.37	1.45	1.49	1.55	1.69				1.67	1.52	1.47	1.43	1.36	1.27	1.17	1.05	0.93	0.81	0.69	0.57	0.50
-3	0.69	0.79	0.94	1.08	1.21	1.31	1.40	1.45	1.50	1.67				1.65	1.47	1.42	1.36	1.28	1.19	1.09	0.98	0.87	0.75	0.64	0.53	0.45
-4	0.68	0.76	0.89	1.03	1.15	1.25	1.33	1.39	1.44	1.57				1.55	1.40	1.33	1.28	1.20	1.09	0.99	0.89	0.78	0.67	0.57	0.47	0.40
-5		0.73	0.82	0.96	1.08	1.18	1.26	1.32	1.36	1.41	1.50	1.54	1.49	1.40	1.32	1.26	1.20	1.11	1.00	0.89	0.79	0.69	0.59	0.49	0.41	0.36
-6		0.67	0.75	0.88	0.99	1.09	1.18	1.24	1.26	1.28	1.26	1.28	1.29	1.26	1.23	1.17	1.09	1.00	0.89	0.79	0.69	0.59	0.49	0.42	0.37	
-7		0.62	0.68	0.78	0.89	0.99	1.08	1.13	1.16	1.18	1.17	1.17	1.18	1.16	1.11	1.05	0.97	0.87	0.73	0.63	0.54	0.46	0.38	0.33		
-8			0.65	0.70	0.79	0.88	0.97	1.03	1.07	1.08	1.09	1.11	1.08	1.06	1.01	0.94	0.87	0.77	0.64	0.54	0.46	0.39	0.33	0.30		
-9				0.65	0.70	0.78	0.85	0.91	0.95	0.98	0.99	1.01	0.98	0.96	0.92	0.86	0.79	0.71	0.62	0.53	0.44	0.38	0.34			
-10					0.65	0.70	0.74	0.79	0.83	0.85	0.87	0.88	0.86	0.84	0.80	0.76	0.70	0.63	0.55	0.48	0.41	0.35				
-11							0.67	0.67	0.70	0.73	0.75	0.73	0.73	0.72	0.69	0.65	0.60	0.54	0.48	0.42	0.37	0.33				
-12								0.59	0.61	0.64	0.66	0.66	0.63	0.63	0.62	0.58	0.54	0.48	0.43	0.38						
-13								0.51					0.59													

Figure 22. Power factors with JEFF 3.2.1 library.

	12	11	10	9	8	7	6	5	4	3	2	1	0	-1	-2	-3	-4	-5	-6	-7	-8	-9	-10	-11	-12	-13
13								0.38	0.36	0.34	0.34	0.34	0.33	0.34	0.36	0.35	0.38	0.38								
12	RELATIVE ERROR [%]							0.34	0.32	0.33	0.31	0.32	0.31	0.32	0.32	0.32	0.33	0.36	0.38	0.39						
11							0.32	0.33	0.31	0.28	0.29	0.27	0.29	0.29	0.29	0.29	0.31	0.33	0.35	0.37	0.40	0.42				
10					0.33	0.31	0.30	0.28	0.28	0.26	0.26	0.28	0.26	0.26	0.26	0.27	0.29	0.30	0.32	0.36	0.37	0.41				
9				0.33	0.31	0.29	0.29	0.26	0.26	0.26	0.25	0.26	0.25	0.25	0.26	0.27	0.28	0.29	0.30	0.33	0.37	0.40	0.42			
8			0.33	0.33	0.30	0.27	0.27	0.25	0.24	0.25	0.24	0.24	0.25	0.24	0.24	0.25	0.25	0.29	0.30	0.34	0.36	0.38	0.42	0.48		
7		0.36	0.33	0.30	0.28	0.27	0.25	0.25	0.23	0.23	0.23	0.24	0.23	0.24	0.24	0.24	0.26	0.26	0.29	0.31	0.35	0.36	0.39	0.44	0.49	
6		0.33	0.31	0.28	0.25	0.26	0.24	0.23	0.23	0.23	0.23	0.22	0.21	0.22	0.23	0.23	0.24	0.25	0.26	0.28	0.31	0.35	0.36	0.40	0.43	
5		0.30	0.30	0.27	0.25	0.24	0.23	0.23	0.23	0.21	0.23	0.22	0.21	0.22	0.21	0.22	0.24	0.24	0.25	0.26	0.29	0.31	0.33	0.37	0.40	
4	0.34	0.31	0.28	0.26	0.25	0.23	0.22	0.23	0.21	0.21	0.21	0.21	0.21	0.21	0.22	0.22	0.23	0.24	0.25	0.26	0.28	0.29	0.31	0.35	0.38	
3	0.32	0.30	0.28	0.26	0.24	0.24	0.21	0.21	0.21	0.21	0.21	0.20	0.21	0.22	0.22	0.22	0.23	0.23	0.24	0.26	0.26	0.28	0.32	0.34	0.37	
2	0.32	0.30	0.26	0.25	0.24	0.23	0.23	0.21	0.21	0.20			0.20	0.21	0.21	0.21	0.21	0.22	0.23	0.25	0.26	0.28	0.29	0.32	0.36	
1	0.32	0.29	0.27	0.25	0.23	0.23	0.23	0.22	0.20					0.21	0.21		0.21	0.22	0.23	0.23	0.25	0.28	0.29	0.32	0.35	
0	0.32	0.29	0.27	0.24	0.24	0.22	0.22	0.22	0.21	0.20			0.20	0.20	0.22	0.21	0.21	0.22	0.23	0.24	0.26	0.28	0.30	0.31	0.35	
-1	0.33	0.30	0.27	0.25	0.24	0.23	0.22	0.22	0.22	0.21	0.19	0.20	0.20	0.22	0.21	0.21	0.21	0.23	0.23	0.24	0.25	0.27	0.31	0.31	0.34	
-2	0.33	0.31	0.27	0.25	0.24	0.23	0.22	0.21	0.22	0.20				0.20	0.22	0.22	0.23	0.23	0.24	0.25	0.26	0.28	0.30	0.34	0.37	
-3	0.34	0.31	0.28	0.26	0.25	0.24	0.23	0.23	0.22	0.21				0.21	0.22	0.22	0.23	0.24	0.25	0.26	0.27	0.29	0.31	0.35	0.39	
-4	0.33	0.32	0.29	0.27	0.26	0.24	0.24	0.23	0.23	0.21				0.22	0.22	0.22	0.24	0.25	0.26	0.27	0.30	0.31	0.33	0.36	0.39	
-5		0.33	0.30	0.27	0.27	0.24	0.24	0.24	0.24	0.24	0.23	0.22	0.23	0.23	0.23	0.23	0.25	0.25	0.27	0.28	0.31	0.34	0.36	0.39	0.42	
-6		0.34	0.33	0.30	0.27	0.27	0.26	0.24	0.24	0.24	0.23	0.24	0.23	0.24	0.24	0.25	0.25	0.27	0.29	0.30	0.32	0.35	0.40	0.41	0.45	
-7		0.36	0.34	0.31	0.29	0.26	0.26	0.27	0.26	0.24	0.25	0.24	0.26	0.26	0.26	0.26	0.27	0.28	0.31	0.35	0.36	0.39	0.43	0.48		
-8			0.35	0.33	0.31	0.29	0.27	0.27	0.27	0.26	0.26	0.27	0.27	0.25	0.27	0.28	0.30	0.30	0.33	0.36	0.41	0.43	0.47	0.48		
-9				0.34	0.33	0.31	0.30	0.28	0.27	0.27	0.28	0.27	0.27	0.28	0.30	0.31	0.31	0.34	0.34	0.37	0.41	0.44	0.49			
-10					0.35	0.34	0.31	0.30	0.31	0.29	0.29	0.29	0.29	0.30	0.31	0.32	0.34	0.33	0.35	0.40	0.43	0.46				
-11							0.34	0.34	0.32	0.32	0.31	0.32	0.32	0.34	0.34	0.35	0.37	0.36	0.40	0.45	0.46	0.47				
-12								0.37	0.34	0.34	0.33	0.34	0.35	0.34	0.36	0.35	0.38	0.40	0.42	0.45						
-13								0.39					0.37													

Figure 23. Relative

The simulation results based on the JEFF-3.2.1 library are listed in

Table 13. The percentage discrepancies defined are related to the difference between the new and the old libraries. As it is showed in Figure 22 the higher power factor is 1.90 and the relative difference to the factor evaluated in the Section 3.5 is 1.57%. Instead the cold channel is remained with the same value.

3.8.1.2 Simulation with JEFF-3.3

Neutronics parameter			with JEFF – 3.3	with ENDF/B - VII.1	Discrepancies
Effective multiplication factor	k_{eff}	[-]	1.00892 ± 0.00005	1.00742 ± 0.00005	0.15 %
Effective delayed neutron fraction	β_{eff}	[pcm]	709 ± 1	687 ± 1	3.10 %
Prompt neutron generation time	Λ_{eff}	[ms]	1.282 ± 0.0004	1.289 ± 0.0003	-0.55 %
Power Normalized Factor	PNF	[n/s]	5.25×10^{16}	5.29×10^{16}	-0.76 %

Table 14. Neutronics parameter with JEFF 3.3 library.

	12	11	10	9	8	7	6	5	4	3	2	1	0	-1	-2	-3	-4	-5	-6	-7	-8	-9	-10	-11	-12	-13
13								0.58	0.59	0.63	0.65	0.68	0.67	0.66	0.64	0.60	0.56	0.52								
12	POWER FACTORS, JEFF 3.3							0.68	0.70	0.73	0.76	0.78	0.77	0.76	0.73	0.68	0.64	0.58	0.54	0.48						
11							0.78	0.79	0.84	0.87	0.90	0.92	0.92	0.90	0.87	0.82	0.76	0.68	0.60	0.53	0.46	0.41				
10					0.73	0.79	0.85	0.92	0.99	1.03	1.05	1.07	1.06	1.04	1.00	0.95	0.88	0.80	0.69	0.60	0.51	0.44				
9				0.72	0.78	0.87	0.98	1.06	1.11	1.15	1.18	1.20	1.19	1.17	1.12	1.06	0.99	0.89	0.77	0.66	0.56	0.47	0.42			
8			0.70	0.77	0.88	0.99	1.10	1.18	1.23	1.26	1.28	1.31	1.30	1.27	1.23	1.17	1.08	0.97	0.81	0.68	0.58	0.48	0.41	0.36		
7		0.66	0.74	0.85	0.98	1.10	1.21	1.28	1.33	1.36	1.35	1.37	1.40	1.37	1.33	1.26	1.17	1.06	0.90	0.77	0.66	0.55	0.46	0.39	0.33	
6		0.71	0.80	0.94	1.08	1.20	1.30	1.38	1.43	1.44	1.43	1.44	1.49	1.47	1.43	1.36	1.27	1.17	1.04	0.92	0.80	0.68	0.56	0.47	0.40	
5		0.77	0.87	1.02	1.16	1.28	1.38	1.45	1.50	1.52	1.53	1.55	1.55	1.53	1.50	1.43	1.36	1.25	1.13	1.01	0.88	0.77	0.65	0.55	0.45	0.39
4	0.69	0.79	0.93	1.08	1.22	1.34	1.43	1.50	1.55	1.57	1.59	1.61	1.59	1.58	1.54	1.49	1.43	1.34	1.21	1.09	0.97	0.85	0.73	0.61	0.50	0.43
3	0.70	0.82	0.97	1.12	1.27	1.38	1.47	1.54	1.59	1.65	1.76	1.78	1.68	1.62	1.58	1.54	1.48	1.40	1.29	1.17	1.05	0.93	0.80	0.68	0.56	0.47
2	0.73	0.84	1.01	1.16	1.29	1.41	1.49	1.56	1.64	1.86			1.86	1.68	1.63	1.64	1.54	1.43	1.33	1.22	1.10	0.97	0.84	0.71	0.59	0.51
1	0.75	0.85	1.02	1.18	1.31	1.42	1.50	1.57	1.71					1.71	1.66		1.61	1.46	1.35	1.25	1.12	1.00	0.86	0.73	0.61	0.53
0	0.75	0.86	1.02	1.17	1.30	1.40	1.49	1.55	1.62	1.82			1.83	1.63	1.59	1.61	1.53	1.44	1.35	1.24	1.12	1.00	0.86	0.73	0.62	0.53
-1	0.74	0.85	1.00	1.15	1.28	1.39	1.47	1.52	1.57	1.67	1.83	1.87	1.74	1.60	1.55	1.52	1.47	1.41	1.32	1.21	1.10	0.98	0.85	0.73	0.60	0.52
-2	0.72	0.83	0.98	1.12	1.26	1.36	1.44	1.50	1.54	1.67				1.66	1.52	1.47	1.42	1.36	1.28	1.17	1.06	0.94	0.82	0.69	0.58	0.50
-3	0.68	0.79	0.94	1.09	1.21	1.32	1.40	1.45	1.50	1.65				1.64	1.47	1.41	1.36	1.29	1.20	1.09	0.98	0.87	0.76	0.64	0.53	0.45
-4	0.67	0.75	0.89	1.03	1.16	1.26	1.34	1.40	1.43	1.56				1.54	1.39	1.33	1.27	1.20	1.10	0.99	0.89	0.78	0.67	0.57	0.47	0.40
-5		0.72	0.82	0.96	1.08	1.19	1.26	1.32	1.36	1.40	1.49	1.53	1.48	1.38	1.31	1.25	1.19	1.11	1.01	0.90	0.79	0.69	0.59	0.49	0.41	0.36
-6		0.67	0.75	0.88	0.99	1.10	1.18	1.24	1.27	1.28	1.27	1.27	1.29	1.26	1.22	1.16	1.09	1.00	0.90	0.79	0.69	0.60	0.49	0.42	0.37	
-7		0.61	0.68	0.79	0.89	0.99	1.08	1.14	1.17	1.18	1.17	1.17	1.18	1.15	1.10	1.03	0.97	0.87	0.73	0.63	0.54	0.46	0.38	0.34		
-8			0.64	0.70	0.79	0.88	0.96	1.03	1.07	1.08	1.10	1.10	1.08	1.06	1.00	0.94	0.87	0.77	0.64	0.54	0.46	0.39	0.33	0.30		
-9				0.64	0.69	0.77	0.84	0.91	0.95	0.97	0.99	1.00	0.99	0.96	0.92	0.86	0.79	0.71	0.61	0.53	0.44	0.38	0.34			
-10					0.64	0.69	0.74	0.78	0.82	0.85	0.86	0.87	0.86	0.83	0.80	0.75	0.69	0.62	0.55	0.47	0.40	0.35				
-11							0.66	0.66	0.69	0.72	0.73	0.74	0.73	0.71	0.68	0.64	0.60	0.54	0.47	0.41	0.36	0.32				
-12								0.57	0.59	0.63	0.65	0.64	0.62	0.62	0.61	0.57	0.53	0.47	0.42	0.37						
-13								0.49					0.57													

Figure 24. Power factors with JEFF 3.3 library.

	12	11	10	9	8	7	6	5	4	3	2	1	0	-1	-2	-3	-4	-5	-6	-7	-8	-9	-10	-11	-12	-13
13								0.38	0.35	0.35	0.35	0.32	0.34	0.34	0.35	0.36	0.39	0.39								
12	RELATIVE ERROR [%]							0.35	0.34	0.33	0.31	0.30	0.31	0.32	0.32	0.33	0.35	0.36	0.39	0.41						
11							0.30	0.30	0.30	0.29	0.29	0.29	0.27	0.28	0.30	0.31	0.31	0.32	0.36	0.37	0.41	0.44				
10					0.33	0.31	0.29	0.29	0.27	0.28	0.28	0.27	0.27	0.27	0.29	0.29	0.31	0.32	0.36	0.39	0.41					
9				0.34	0.31	0.30	0.28	0.28	0.25	0.26	0.26	0.25	0.25	0.26	0.25	0.27	0.28	0.29	0.31	0.33	0.37	0.41	0.43			
8			0.35	0.32	0.31	0.27	0.27	0.26	0.25	0.24	0.24	0.24	0.24	0.24	0.25	0.26	0.27	0.27	0.30	0.33	0.37	0.39	0.43	0.44		
7		0.35	0.33	0.31	0.29	0.27	0.25	0.25	0.24	0.23	0.24	0.23	0.23	0.24	0.24	0.25	0.24	0.27	0.28	0.31	0.33	0.36	0.41	0.42	0.49	
6		0.33	0.31	0.29	0.27	0.25	0.24	0.24	0.23	0.22	0.22	0.23	0.21	0.22	0.23	0.23	0.24	0.25	0.27	0.29	0.29	0.33	0.35	0.40	0.44	
5		0.31	0.29	0.28	0.26	0.25	0.23	0.22	0.23	0.23	0.21	0.21	0.22	0.21	0.23	0.22	0.23	0.25	0.27	0.28	0.29	0.32	0.32	0.36	0.41	
4	0.31	0.32	0.28	0.27	0.24	0.24	0.23	0.22	0.21	0.21	0.21	0.21	0.22	0.22	0.22	0.22	0.23	0.23	0.25	0.27	0.26	0.30	0.31	0.34	0.38	
3	0.33	0.30	0.28	0.26	0.24	0.23	0.22	0.23	0.21	0.21	0.20	0.19	0.20	0.21	0.22	0.22	0.23	0.23	0.24	0.26	0.27	0.29	0.30	0.33	0.35	
2	0.32	0.30	0.26	0.25	0.23	0.23	0.22	0.22	0.21	0.20			0.19	0.21	0.21	0.21	0.22	0.22	0.25	0.24	0.26	0.28	0.29	0.33	0.36	
1	0.32	0.29	0.26	0.24	0.24	0.22	0.22	0.21	0.22					0.20	0.22		0.21	0.23	0.23	0.25	0.27	0.27	0.30	0.32	0.36	
0	0.31	0.29	0.27	0.26	0.23	0.22	0.22	0.22	0.21	0.20			0.20	0.20	0.21	0.21	0.21	0.22	0.23	0.24	0.25	0.28	0.29	0.31	0.36	
-1	0.32	0.30	0.26	0.26	0.24	0.23	0.23	0.21	0.21	0.21	0.20	0.21	0.20	0.22	0.21	0.22	0.22	0.23	0.23	0.24	0.25	0.28	0.31	0.31	0.34	
-2	0.33	0.31	0.27	0.25	0.24	0.24	0.23	0.22	0.22	0.21				0.21	0.22	0.23	0.22	0.23	0.24	0.25	0.26	0.29	0.31	0.32	0.35	
-3	0.35	0.31	0.27	0.25	0.25	0.24	0.23	0.22	0.22	0.21				0.21	0.22	0.22	0.23	0.24	0.25	0.26	0.27	0.29	0.31	0.34	0.39	
-4	0.33	0.32	0.29	0.28	0.25	0.25	0.24	0.23	0.23	0.22				0.22	0.23	0.23	0.24	0.24	0.25	0.27	0.28	0.30	0.34	0.37	0.40	
-5		0.33	0.30	0.27	0.28	0.26	0.24	0.24	0.23	0.23	0.22	0.22	0.22	0.24	0.23	0.25	0.25	0.26	0.28	0.28	0.31	0.33	0.36	0.37	0.42	
-6		0.34	0.33	0.30	0.28	0.27	0.26	0.25	0.24	0.23	0.24	0.25	0.24	0.26	0.25	0.27	0.26	0.26	0.28	0.31	0.32	0.35	0.39	0.42	0.45	
-7		0.37	0.33	0.32	0.30	0.27	0.26	0.25	0.26	0.25	0.25	0.25	0.25	0.26	0.27	0.26	0.28	0.30	0.32	0.34	0.37	0.39	0.44	0.46		
-8			0.36	0.34	0.31	0.30	0.29	0.28	0.26	0.27	0.26	0.26	0.28	0.27	0.27	0.28	0.29	0.31	0.33	0.36	0.41	0.42	0.47	0.52		
-9				0.35	0.35	0.33	0.31	0.29	0.28	0.28	0.28	0.28	0.28	0.27	0.29	0.30	0.31	0.33	0.33	0.39	0.42	0.46	0.47			
-10					0.37	0.34	0.33	0.31	0.30	0.30	0.30	0.29	0.30	0.30	0.32	0.32	0.32	0.35	0.37	0.38	0.43	0.47				
-11							0.36	0.34	0.33	0.34	0.31	0.31	0.33	0.33	0.35	0.36	0.37	0.39	0.41	0.43	0.46	0.49				
-12								0.36	0.37	0.36	0.34	0.35	0.36	0.36	0.37	0.37	0.39	0.43	0.43	0.47						
-13								0.41					0.37													

Figure 25. Relative error evaluated with JEFF

With JEFF-3.3 library, we have the highest effective delayed neutron fraction β_{eff} discrepancy (3.10%) than the other values obtained with the different libraries. About the power factors, both the highest and lowest values are the same than the ones obtained with ENDF-71. The small differences are in the statistical errors that in this case respectively are 0.21% and 0.52%.

3.8.1.3 Simulation with JENDL-4.0u

Neutronics parameter			with JENDL-4.0u	with ENDF/B - VII.1	Discrepancies
Effective multiplication factor	k_{eff}	[-]	1.00680 ± 0.00005	1.00742 ± 0.00005	-0.07 %
Effective delayed neutron fraction	β_{eff}	[pcm]	693 ± 1	687 ± 1	0.87 %
Prompt neutron generation time	Λ_{eff}	[ms]	1.290 ± 0.0004	1.289 ± 0.0003	0.08 %
Power Normalized Factor	PNF	[n/s]	5.29×10^{16}	5.29×10^{16}	0.00 %

Table 15. Neutronics parameter with JENDL-4.0u library.

	12	11	10	9	8	7	6	5	4	3	2	1	0	-1	-2	-3	-4	-5	-6	-7	-8	-9	-10	-11	-12	-13
13								0.57	0.59	0.62	0.66	0.67	0.67	0.66	0.63	0.60	0.56	0.52								
12	POWER FACTORS, JENDL-40u							0.67	0.69	0.72	0.75	0.77	0.77	0.76	0.73	0.69	0.64	0.59	0.54	0.49						
11							0.77	0.78	0.83	0.86	0.90	0.92	0.91	0.90	0.87	0.82	0.76	0.69	0.61	0.53	0.47	0.41				
10					0.73	0.79	0.85	0.91	0.97	1.00	1.04	1.07	1.06	1.04	1.00	0.95	0.88	0.80	0.70	0.60	0.51	0.45				
9				0.71	0.78	0.86	0.96	1.04	1.11	1.14	1.17	1.20	1.19	1.17	1.12	1.07	0.99	0.89	0.78	0.67	0.56	0.48	0.42			
8			0.70	0.76	0.87	0.98	1.08	1.16	1.22	1.25	1.28	1.30	1.30	1.27	1.23	1.16	1.08	0.97	0.82	0.69	0.59	0.49	0.41	0.36		
7		0.65	0.73	0.85	0.97	1.09	1.19	1.27	1.33	1.34	1.34	1.37	1.38	1.37	1.33	1.27	1.18	1.06	0.90	0.77	0.67	0.56	0.47	0.39	0.34	
6		0.70	0.80	0.94	1.07	1.19	1.29	1.37	1.42	1.44	1.42	1.44	1.47	1.46	1.43	1.36	1.28	1.17	1.05	0.93	0.81	0.69	0.57	0.47	0.41	
5		0.76	0.86	1.01	1.14	1.26	1.37	1.44	1.49	1.51	1.52	1.55	1.54	1.52	1.49	1.43	1.36	1.26	1.15	1.02	0.91	0.78	0.66	0.55	0.46	0.40
4	0.69	0.78	0.92	1.07	1.21	1.33	1.43	1.49	1.54	1.57	1.59	1.61	1.59	1.57	1.54	1.50	1.42	1.34	1.22	1.10	0.98	0.86	0.74	0.63	0.51	0.44
3	0.70	0.81	0.97	1.12	1.25	1.37	1.46	1.52	1.58	1.65	1.76	1.78	1.67	1.61	1.58	1.54	1.48	1.40	1.29	1.18	1.07	0.94	0.81	0.69	0.56	0.49
2	0.73	0.84	1.00	1.15	1.28	1.40	1.48	1.55	1.64	1.85			1.86	1.67	1.63	1.63	1.54	1.44	1.34	1.23	1.11	0.98	0.85	0.73	0.60	0.52
1	0.74	0.85	1.01	1.16	1.30	1.40	1.48	1.56	1.70					1.71	1.66		1.60	1.45	1.36	1.26	1.14	1.01	0.86	0.74	0.62	0.54
0	0.75	0.85	1.01	1.16	1.30	1.40	1.48	1.54	1.62	1.83			1.82	1.63	1.59	1.62	1.53	1.44	1.35	1.24	1.13	1.01	0.86	0.74	0.62	0.54
-1	0.73	0.84	1.00	1.15	1.28	1.38	1.46	1.52	1.56	1.66	1.83	1.87	1.73	1.60	1.54	1.52	1.47	1.41	1.32	1.22	1.10	0.98	0.86	0.73	0.61	0.53
-2	0.71	0.82	0.97	1.12	1.25	1.36	1.44	1.48	1.53	1.67				1.66	1.52	1.47	1.43	1.37	1.28	1.18	1.07	0.95	0.82	0.70	0.58	0.50
-3	0.68	0.78	0.93	1.08	1.20	1.30	1.39	1.44	1.49	1.65				1.64	1.47	1.42	1.37	1.30	1.21	1.10	1.00	0.87	0.76	0.64	0.53	0.46
-4	0.66	0.75	0.88	1.02	1.14	1.25	1.33	1.38	1.42	1.56				1.54	1.40	1.34	1.28	1.20	1.11	1.00	0.90	0.79	0.68	0.57	0.47	0.40
-5		0.72	0.82	0.95	1.07	1.17	1.25	1.31	1.35	1.40	1.49	1.53	1.49	1.38	1.32	1.26	1.20	1.11	1.01	0.90	0.80	0.69	0.59	0.50	0.42	0.36
-6		0.66	0.75	0.87	0.99	1.09	1.17	1.23	1.27	1.28	1.27	1.27	1.29	1.27	1.22	1.16	1.10	1.00	0.90	0.80	0.69	0.59	0.49	0.42	0.37	
-7		0.61	0.67	0.78	0.89	0.99	1.07	1.13	1.17	1.17	1.16	1.17	1.17	1.15	1.11	1.04	0.97	0.87	0.74	0.63	0.55	0.46	0.39	0.34		
-8			0.64	0.70	0.79	0.88	0.96	1.02	1.06	1.08	1.09	1.10	1.09	1.06	1.01	0.95	0.87	0.78	0.65	0.55	0.46	0.39	0.33	0.30		
-9				0.65	0.69	0.77	0.84	0.91	0.95	0.98	0.99	1.00	0.99	0.96	0.92	0.86	0.80	0.72	0.62	0.53	0.45	0.38	0.34			
-10					0.64	0.69	0.73	0.78	0.82	0.85	0.87	0.88	0.86	0.84	0.81	0.76	0.70	0.63	0.55	0.48	0.41	0.36				
-11							0.67	0.66	0.69	0.72	0.74	0.75	0.74	0.72	0.70	0.65	0.60	0.54	0.48	0.42	0.36	0.33				
-12								0.57	0.60	0.63	0.66	0.65	0.63	0.63	0.61	0.57	0.53	0.48	0.42	0.38						
-13								0.50					0.57													

Figure 26. Power factors with JENDL-4.0u library.

	12	11	10	9	8	7	6	5	4	3	2	1	0	-1	-2	-3	-4	-5	-6	-7	-8	-9	-10	-11	-12	-13
13								0.38	0.36	0.35	0.34	0.32	0.35	0.34	0.35	0.38	0.38	0.39								
12	RELATIVE ERROR [%]							0.35	0.33	0.33	0.31	0.32	0.31	0.31	0.31	0.34	0.33	0.37	0.37							
11							0.32	0.31	0.30	0.30	0.28	0.30	0.29	0.29	0.30	0.32	0.31	0.33	0.36	0.39	0.40	0.43				
10					0.33	0.31	0.30	0.29	0.28	0.27	0.27	0.27	0.25	0.27	0.27	0.28	0.29	0.30	0.32	0.35	0.38	0.42				
9				0.33	0.31	0.30	0.28	0.27	0.27	0.25	0.26	0.25	0.25	0.24	0.26	0.28	0.27	0.28	0.29	0.32	0.35	0.39	0.44			
8			0.33	0.31	0.30	0.29	0.26	0.26	0.25	0.23	0.24	0.23	0.24	0.24	0.26	0.26	0.29	0.31	0.32	0.34	0.38	0.41	0.44			
7		0.35	0.32	0.29	0.28	0.27	0.25	0.24	0.24	0.23	0.24	0.22	0.24	0.22	0.23	0.24	0.24	0.26	0.29	0.30	0.33	0.36	0.39	0.45	0.48	
6		0.33	0.30	0.28	0.26	0.25	0.23	0.23	0.24	0.23	0.22	0.22	0.22	0.23	0.22	0.23	0.24	0.25	0.26	0.28	0.30	0.32	0.35	0.40	0.42	
5		0.31	0.29	0.28	0.25	0.23	0.23	0.21	0.22	0.22	0.22	0.22	0.22	0.21	0.23	0.22	0.24	0.24	0.25	0.27	0.29	0.30	0.35	0.35	0.41	0.44
4	0.34	0.30	0.28	0.26	0.26	0.23	0.22	0.22	0.22	0.21	0.21	0.20	0.21	0.21	0.22	0.22	0.22	0.22	0.24	0.26	0.28	0.28	0.31	0.35	0.38	0.42
3	0.32	0.30	0.28	0.26	0.24	0.23	0.22	0.21	0.21	0.20	0.21	0.20	0.21	0.20	0.20	0.21	0.22	0.23	0.23	0.25	0.26	0.28	0.31	0.31	0.36	0.40
2	0.32	0.29	0.27	0.25	0.24	0.24	0.21	0.22	0.21	0.20			0.20	0.20	0.20	0.20	0.21	0.22	0.24	0.24	0.25	0.27	0.30	0.31	0.35	0.40
1	0.33	0.31	0.27	0.25	0.23	0.23	0.21	0.21	0.22					0.21	0.20		0.22	0.22	0.24	0.24	0.26	0.28	0.29	0.32	0.33	0.39
0	0.33	0.30	0.29	0.26	0.23	0.23	0.22	0.22	0.21	0.20			0.21	0.21	0.21	0.21	0.23	0.23	0.24	0.24	0.26	0.27	0.29	0.31	0.36	0.38
-1	0.32	0.30	0.26	0.25	0.24	0.23	0.22	0.23	0.22	0.21	0.21	0.20	0.21	0.22	0.21	0.22	0.22	0.23	0.23	0.24	0.25	0.27	0.28	0.32	0.34	0.37
-2	0.33	0.29	0.28	0.25	0.24	0.24	0.23	0.22	0.23	0.21				0.20	0.22	0.22	0.23	0.23	0.23	0.24	0.27	0.28	0.31	0.33	0.35	0.40
-3	0.33	0.32	0.27	0.26	0.25	0.24	0.23	0.23	0.22	0.21				0.22	0.22	0.23	0.23	0.23	0.25	0.25	0.26	0.28	0.31	0.34	0.38	0.41
-4	0.35	0.30	0.28	0.28	0.25	0.25	0.24	0.23	0.22	0.21				0.22	0.22	0.24	0.24	0.24	0.26	0.28	0.28	0.30	0.32	0.36	0.39	0.44
-5		0.32	0.29	0.28	0.26	0.25	0.25	0.25	0.24	0.23	0.22	0.22	0.22	0.23	0.23	0.24	0.24	0.24	0.26	0.27	0.28	0.30	0.32	0.36	0.39	0.46
-6		0.33	0.33	0.28	0.28	0.26	0.26	0.26	0.24	0.23	0.24	0.24	0.24	0.24	0.24	0.25	0.25	0.25	0.27	0.29	0.30	0.33	0.34	0.39	0.42	0.46
-7		0.36	0.34	0.30	0.29	0.27	0.26	0.26	0.23	0.24	0.24	0.25	0.25	0.25	0.25	0.27	0.27	0.29	0.32	0.34	0.37	0.39	0.44	0.46		
-8			0.34	0.34	0.30	0.28	0.28	0.27	0.26	0.27	0.26	0.26	0.25	0.26	0.27	0.27	0.28	0.31	0.32	0.36	0.41	0.44	0.49	0.50		
-9				0.35	0.34	0.31	0.28	0.28	0.28	0.28	0.27	0.28	0.28	0.28	0.29	0.30	0.31	0.33	0.35	0.38	0.42	0.44	0.46			
-10					0.35	0.33	0.33	0.30	0.30	0.29	0.30	0.29	0.30	0.31	0.31	0.31	0.34	0.35	0.37	0.39	0.44	0.46				
-11							0.34	0.34	0.31	0.33	0.32	0.32	0.32	0.32	0.33	0.35	0.37	0.38	0.42	0.43	0.46	0.48				
-12								0.35	0.36	0.35	0.35	0.35	0.35	0.35	0.36	0.38	0.39	0.42	0.41	0.46						
-13								0.40					0.37													

Figure 27. Relative error evaluated with JENDL-4.0u library.

The greatest affinity with the ENDF/B-VII.1 library is with JENDL-4.0u one. Here the percentage discrepancies are very low for all neutronic parameters, PNF and power factor.

3.8.1.4 Simulation with ENDF/B-VIII.0

Neutronics parameter			with ENDF/B-VIII.0	with ENDF/B - VII.1	Discrepancies
Effective multiplication factor	k_{eff}	[-]	1.01030 ± 0.00005	1.00742 ± 0.00005	0.29 %
Effective delayed neutron fraction	β_{eff}	[pcm]	691 ± 1	687 ± 1	0.58 %
Prompt neutron generation time	Λ_{eff}	[ms]	1.277 ± 0.0004	1.289 ± 0.0003	-0.94 %
Power Normalized Factor	PNF	[n/s]	5.24×10^{16}	5.29×10^{16}	-0.95 %

Table 16. Neutronics parameter with ENDF/B-VIII.0 library.

	12	11	10	9	8	7	6	5	4	3	2	1	0	-1	-2	-3	-4	-5	-6	-7	-8	-9	-10	-11	-12	-13
13								0,57	0,58	0,62	0,65	0,66	0,67	0,66	0,63	0,60	0,56	0,52								
12	POWER FACTORS, ENDF/B-VIII.0							0,67	0,68	0,72	0,75	0,77	0,77	0,75	0,73	0,69	0,64	0,59	0,54	0,49						
11							0,77	0,78	0,82	0,86	0,89	0,92	0,91	0,90	0,86	0,82	0,75	0,69	0,61	0,53	0,46	0,41				
10					0,72	0,78	0,84	0,91	0,97	1,01	1,04	1,06	1,05	1,03	1,00	0,94	0,87	0,80	0,70	0,60	0,51	0,44				
9				0,72	0,77	0,87	0,96	1,04	1,10	1,14	1,17	1,20	1,18	1,16	1,13	1,07	0,99	0,88	0,77	0,66	0,56	0,47	0,42			
8			0,69	0,77	0,87	0,99	1,09	1,17	1,23	1,25	1,28	1,30	1,29	1,27	1,23	1,16	1,08	0,96	0,81	0,68	0,58	0,48	0,40	0,35		
7		0,66	0,73	0,85	0,98	1,09	1,20	1,28	1,33	1,35	1,34	1,36	1,38	1,37	1,32	1,26	1,17	1,06	0,89	0,76	0,65	0,55	0,45	0,38	0,34	
6		0,71	0,80	0,94	1,07	1,19	1,30	1,37	1,43	1,44	1,43	1,44	1,47	1,46	1,43	1,36	1,27	1,16	1,04	0,92	0,79	0,67	0,56	0,47	0,40	
5		0,76	0,88	1,02	1,15	1,27	1,37	1,45	1,50	1,51	1,53	1,55	1,54	1,52	1,49	1,43	1,35	1,25	1,13	1,01	0,89	0,77	0,65	0,54	0,45	0,39
4	0,70	0,79	0,93	1,08	1,22	1,34	1,43	1,50	1,55	1,57	1,60	1,61	1,59	1,57	1,55	1,49	1,42	1,32	1,21	1,09	0,97	0,86	0,73	0,61	0,50	0,42
3	0,71	0,81	0,97	1,13	1,26	1,38	1,48	1,54	1,59	1,66	1,76	1,78	1,68	1,61	1,58	1,54	1,47	1,38	1,28	1,17	1,05	0,92	0,80	0,67	0,55	0,47
2	0,73	0,84	1,00	1,16	1,29	1,41	1,50	1,57	1,65	1,86			1,86	1,66	1,64	1,63	1,53	1,43	1,32	1,22	1,10	0,97	0,84	0,71	0,59	0,51
1	0,75	0,85	1,02	1,17	1,32	1,43	1,51	1,58	1,71					1,71	1,67		1,59	1,45	1,35	1,24	1,13	0,99	0,86	0,73	0,61	0,53
0	0,75	0,86	1,02	1,17	1,30	1,41	1,50	1,55	1,62	1,83			1,83	1,63	1,58	1,61	1,53	1,43	1,34	1,23	1,12	0,99	0,85	0,73	0,61	0,53
-1	0,74	0,85	1,01	1,15	1,29	1,40	1,47	1,52	1,56	1,66	1,84	1,87	1,74	1,60	1,55	1,52	1,47	1,40	1,31	1,21	1,10	0,97	0,85	0,72	0,60	0,52
-2	0,72	0,83	0,98	1,13	1,26	1,37	1,44	1,50	1,54	1,68				1,66	1,52	1,48	1,43	1,36	1,27	1,17	1,06	0,94	0,81	0,69	0,57	0,49
-3	0,69	0,79	0,94	1,09	1,22	1,32	1,41	1,46	1,50	1,66				1,65	1,47	1,41	1,36	1,29	1,20	1,09	0,99	0,87	0,75	0,63	0,52	0,45
-4	0,67	0,75	0,89	1,03	1,16	1,27	1,35	1,39	1,43	1,57				1,55	1,40	1,34	1,28	1,21	1,10	1,00	0,88	0,78	0,67	0,56	0,46	0,40
-5		0,72	0,83	0,96	1,08	1,19	1,28	1,33	1,36	1,41	1,50	1,54	1,50	1,39	1,31	1,26	1,20	1,11	1,00	0,90	0,79	0,68	0,58	0,49	0,41	0,36
-6		0,67	0,75	0,88	1,00	1,10	1,19	1,25	1,28	1,29	1,27	1,28	1,29	1,27	1,22	1,16	1,10	1,00	0,90	0,79	0,69	0,59	0,49	0,41	0,37	
-7		0,62	0,68	0,79	0,90	1,00	1,09	1,14	1,18	1,19	1,17	1,18	1,18	1,16	1,11	1,05	0,97	0,87	0,74	0,64	0,54	0,46	0,38	0,33		
-8			0,64	0,70	0,80	0,89	0,98	1,04	1,07	1,09	1,10	1,11	1,09	1,06	1,01	0,95	0,87	0,78	0,65	0,54	0,46	0,39	0,33	0,29		
-9				0,65	0,70	0,78	0,86	0,92	0,96	0,98	1,00	1,01	0,99	0,96	0,92	0,86	0,80	0,72	0,62	0,53	0,45	0,38	0,33			
-10					0,65	0,69	0,74	0,79	0,84	0,86	0,88	0,88	0,87	0,84	0,80	0,75	0,70	0,63	0,56	0,47	0,40	0,35				
-11						0,67	0,67	0,71	0,72	0,74	0,75	0,74	0,72	0,69	0,65	0,60	0,54	0,48	0,41	0,37	0,32					
-12							0,57	0,61	0,64	0,65	0,66	0,63	0,63	0,61	0,58	0,54	0,48	0,42	0,38							
-13							0,50						0,58													

Figure 28. Power factors with ENDF/B-VIII.0 library.

	12	11	10	9	8	7	6	5	4	3	2	1	0	-1	-2	-3	-4	-5	-6	-7	-8	-9	-10	-11	-12	-13
13								0.37	0.37	0.36	0.36	0.33	0.35	0.33	0.35	0.36	0.38	0.39								
12	RELATIVE ERROR [%]							0.34	0.33	0.32	0.31	0.32	0.31	0.31	0.31	0.32	0.34	0.37	0.37	0.41						
11							0.32	0.33	0.29	0.29	0.30	0.30	0.29	0.29	0.29	0.29	0.31	0.33	0.36	0.38	0.42	0.43				
10					0.33	0.32	0.29	0.28	0.28	0.27	0.27	0.27	0.26	0.26	0.28	0.28	0.29	0.30	0.32	0.35	0.38	0.42				
9				0.33	0.32	0.31	0.28	0.29	0.26	0.27	0.25	0.25	0.25	0.26	0.25	0.26	0.27	0.28	0.32	0.35	0.36	0.41	0.42			
8			0.33	0.32	0.30	0.29	0.27	0.25	0.24	0.24	0.24	0.25	0.24	0.24	0.25	0.26	0.26	0.27	0.31	0.34	0.36	0.40	0.42	0.47		
7		0.35	0.32	0.29	0.28	0.26	0.25	0.24	0.24	0.23	0.23	0.23	0.23	0.23	0.23	0.24	0.25	0.27	0.29	0.31	0.34	0.35	0.39	0.44	0.45	
6		0.33	0.29	0.28	0.26	0.25	0.23	0.24	0.23	0.22	0.22	0.22	0.23	0.21	0.23	0.23	0.24	0.26	0.26	0.28	0.31	0.35	0.35	0.39	0.41	
5		0.33	0.30	0.27	0.25	0.25	0.23	0.23	0.23	0.22	0.22	0.21	0.21	0.23	0.22	0.23	0.24	0.24	0.26	0.26	0.29	0.32	0.33	0.37	0.39	
4	0.35	0.31	0.29	0.25	0.25	0.23	0.22	0.22	0.22	0.21	0.21	0.21	0.21	0.20	0.22	0.23	0.23	0.24	0.25	0.26	0.28	0.30	0.32	0.35	0.37	
3	0.34	0.31	0.28	0.26	0.24	0.23	0.22	0.22	0.22	0.22	0.20	0.21	0.20	0.21	0.22	0.21	0.22	0.23	0.24	0.25	0.27	0.28	0.30	0.32	0.37	
2	0.32	0.30	0.27	0.26	0.25	0.23	0.22	0.22	0.21	0.20			0.19	0.21	0.21	0.21	0.21	0.23	0.23	0.25	0.27	0.27	0.28	0.32	0.35	
1	0.32	0.30	0.28	0.26	0.24	0.23	0.22	0.21	0.21					0.20	0.21		0.21	0.23	0.23	0.24	0.26	0.27	0.29	0.33	0.35	
0	0.33	0.30	0.27	0.25	0.24	0.24	0.21	0.22	0.21	0.20			0.20	0.21	0.21	0.22	0.22	0.22	0.24	0.24	0.26	0.28	0.30	0.32	0.35	
-1	0.32	0.29	0.27	0.26	0.24	0.24	0.22	0.22	0.21	0.20	0.21	0.20	0.21	0.21	0.22	0.21	0.22	0.22	0.23	0.24	0.26	0.29	0.31	0.33	0.34	
-2	0.33	0.31	0.28	0.27	0.24	0.24	0.23	0.21	0.22	0.20				0.20	0.21	0.22	0.22	0.24	0.24	0.25	0.27	0.29	0.30	0.33	0.36	
-3	0.34	0.31	0.28	0.26	0.25	0.25	0.23	0.22	0.22	0.21				0.21	0.23	0.23	0.24	0.24	0.25	0.25	0.28	0.29	0.32	0.33	0.38	
-4	0.35	0.32	0.29	0.26	0.25	0.24	0.24	0.23	0.23	0.21				0.22	0.23	0.23	0.24	0.25	0.26	0.28	0.29	0.31	0.33	0.35	0.41	
-5		0.34	0.30	0.27	0.26	0.25	0.25	0.23	0.24	0.23	0.22	0.22	0.23	0.22	0.23	0.25	0.24	0.25	0.26	0.30	0.30	0.32	0.34	0.39	0.41	
-6		0.33	0.31	0.29	0.27	0.27	0.26	0.25	0.24	0.24	0.24	0.24	0.24	0.24	0.24	0.25	0.25	0.26	0.27	0.28	0.30	0.32	0.35	0.40	0.41	
-7		0.35	0.33	0.33	0.29	0.27	0.27	0.26	0.25	0.26	0.25	0.25	0.25	0.25	0.27	0.27	0.28	0.28	0.32	0.34	0.37	0.38	0.42	0.46		
-8			0.34	0.33	0.31	0.30	0.28	0.28	0.27	0.27	0.27	0.27	0.26	0.26	0.27	0.27	0.28	0.31	0.33	0.36	0.41	0.43	0.48	0.50		
-9				0.35	0.34	0.32	0.30	0.30	0.28	0.27	0.28	0.27	0.27	0.28	0.28	0.30	0.31	0.32	0.34	0.37	0.42	0.44	0.48			
-10					0.34	0.35	0.34	0.31	0.31	0.29	0.29	0.30	0.30	0.30	0.31	0.32	0.33	0.35	0.37	0.41	0.43	0.46				
-11							0.36	0.34	0.33	0.32	0.34	0.33	0.32	0.33	0.34	0.35	0.36	0.37	0.40	0.43	0.45	0.49				
-12								0.38	0.36	0.35	0.34	0.34	0.34	0.36	0.37	0.37	0.38	0.41	0.44	0.45						
-13								0.40					0.38													

Figure 29. Relative error evaluated

The last different library used is the ENDF/B-VIII.0. As we can observe in the last column of Table 16, also in this case the differences with the previously used library are very low. The minimum value of the power factor is 0.29 against the 0.30 of the ENDF/B-VIII.0 library.

3.8.2 Impact of fuel burn up

The main assumption on the base of these analysis is to consider the entire nuclear fuel as fresh metallic fuel with the only isotopes of U234, U235 and U238. Actually in the BR1 the nuclear fuel has never been changed so the composition is different according to the burnup. However, we know that the power level of the reactor has always been very low compared to any other thermal reactor. The change of composition fuel occurred but it is not predominant for the conditioning of the calculations. In this section we want to demonstrate the impact of the burnup for the BR1 reactor. In order to do that, the fuel material composition is choose in as more conservative as possible in terms of U235 burning. The fuel with the minor amount of U235 dates back to 1957 that also includes the minor actinides and fission products. Here the fraction of U235 is 0.66% and if we consider the same volume of the fresh fuel, the difference is 8.76%.

Hence, the simulation is performed considering the entire core loaded with this depleted fuel and the main neutronics parameters are evaluated.

Neutronics parameter			Fresh fuel	Depleted fuel	Discrepancies
Effective multiplication factor	k_{eff}	[-]	1.01030 ± 5 [pcm]	1.01009 ± 5 [pcm]	0.02 %
Effective delayed neutron fraction	β_{eff}	[pcm]	691 ± 1	638 ± 1	7.67 %
Prompt neutron generation time	Λ_{eff}	[ms]	1.277 ± 0.0004	1.243 ± 0.0004	2.66 %
Power Normalized Factor	PNF	[n/s]	5.24×10^{16}	5.36×10^{16}	-2.29 %

			PF	$\Delta_{rel}\%$	PF	$\Delta_{rel}\%$	
Power factor of the hot channel	PF _{MAX}	[-]	1.877	0.199	1.863	0.201	0.75 %
Power factor of the cold channel	PF _{MIN}	[-]	0.294	0.525	0.297	0.507	-1.02 %

Table 17. Comparison between fresh and depleted fuel.

The adoption of the depleted fuel in as more conservative as possible way leads a reduced discrepancies on the main neutronic parameters than the fresh fuel. Hence, from the results obtained we can state that the impact of the fuel burn up for this reactor is not a predominant factor that conditions the main parameters.

Conclusions

This study presents the develop of the neutron model of the BR1 reactor with the Serpent code starting from the geometric construction of the input to the evaluation of the main parameters that govern the neutron nature of the reactor.

The BR1 reactor was the first nuclear reactor ever built in Belgium, in operation since 1956. It is cooled by forced air convection, moderated by graphite and fed with natural metallic uranium. Support for BR1 testing and calibration programs was provided by the particle transport code MCNP. It represents one of the most widespread codes in nuclear applications. This experience guarantees safety and reliability of use.

This work arises from the need to model BR1 with a new neutron transport computation code to offer greater flexibility, reliability and diversification of the evaluation tools. The new calculation code to be introduced must be subjected to a phase of validation of the simulated model which implies a comparison with experimental data and results of models in use. Once the input code in Serpent of the BR1 reactor was built, the simulations carried out provided results that were compared with data obtained with MCNP. However, the Serpent code offers several advantages from a compilation point of view. The treatment of the energy grid that is the same for all nuclides and the combination of the conventional surface-tracking and the Woodcock delta-tracking method are some of the improvements adopted to streamline simulation times. In addition, the Serpent code has a more intuitive programming language which allows for better interpretation of the input files.

The first objective was to build the reactor geometry by adopting a modular approach. Each element has been made independently so as to be able to organize the overall geometry in the best possible way. The first modules created were the fuel rod, the moderator and the control rod. Subsequently, the core was inserted inside a biological shielding in concrete surrounded by a layer of air. The geometry was concluded with the introduction of two thermal columns, vertical and horizontal.

Once the geometric construction of the BR1 was defined, nuclear evaluations were performed on the main neutron indicators. The nuclear parameters including the effective multiplication factor k_{eff} and the effective delayed neutron fraction β_{eff} were obtained directly from the analysis of the code output file. While the neutron spectrum, the flux distribution, the reaction rates and the power maps were obtained through the post processing of the results of the various defined detectors. Each quantity obtained is associated with a purely statistical relative error without considering other sources of uncertainty (e.g. nuclear data). The results are consistent with previous studies based on the MCNP code in quantitative terms and with compatible levels of accuracy.

To assess the impact of the main assumptions that have been adopted, a sensitivity analysis was conducted. In particular, the JEFF-3.1.1 nuclear data library is used in the MCNP code which is not available for Serpent for which the ENDF/B-VII.1 library has been adopted. Therefore, the first part of the sensitivity analysis was conducted to assess the impact on the main nuclear indicators of some data libraries (JEFF-3.1.2, JEFF-3.3, JENDL-4.0u and ENDF/B-VIII.0). The results of the comparison have an insubstantial impact on the main parameters so the use of the ENDF/B-VII.1 library does not particularly affect the analysis of the Serpent code.

The other important assumption is the introduction of fresh nuclear fuel throughout the core. The BR1 has never replaced the fuel as the power and burnup values are so low that they have a low impact on neutron fluxes. Therefore, the analysis was conducted to demonstrate that the fuel assumption is realistic. The discrepancies between the condition in which the core is loaded with the highest burnup fuel (as conservative as possible) and the simulation with fresh fuel demonstrate the low impact on the main nuclear parameters.

The values obtained from the modeling of the BR1 reactor through the Serpent code show compatibility with respect to the characterization with the MCNP model. The capability to obtain simulations with good accuracy and relatively low computational cost are features that promise future use of the new code in this application. Finally, the validation phase must be completed with studies on other neutron indicators of the reactor. The analysis of the reaction rates inside the thermal columns, the characterization of the neutron spectrum in the empty big cavity and with the MARK-III converter, the evaluation of the photon spectrum, the activation of argon and graphite, the simulation of fuel depletion are some of the further studies that need to be conducted to get full feedback on the new code.

References

- [1] E. Malambu, "A thorough characterization of the neutron-photon fields in the SCK CEN BR1 research reactor," SCK CEN, Mol - Belgium, 2016.
- [2] A. Haghghat, Monte Carlo methods for particle transport, S. Edition, Ed., CRC Press, Taylor & Francis Group, 2021.
- [3] J. J. Duderstadt and L. J. Hamilton, "Nuclear-Reactor Analysis," John Wiley & sons, inc, Michigan, 1976.
- [4] A. Hellander, "Stochastic Simulation and Monte Carlo Methods," 2009.
- [5] J. R. Lamarsh and A. J. Baratta, Introduction to Nuclear Engineering, vol. Third Edit, Prentice-Hall, Inc., 2001.
- [6] VTT, "Serpent - a Continuous-energy Monte Carlo Reactor Physics Burnup Calculation," [Online]. Available: <http://montecarlo.vtt.fi/index.htm>.
- [7] J. Leppänen, Development of a New Monte Carlo Reactor Physics Code, Edita Prima Oy, Helsinki 2007, 2007, pp. 3-228.
- [8] A. Trkov, "From Basic Nuclear Data to Applications," Ljubljana, Slovenia, 2000.
- [9] C. J. Lloyd and P. Romano, "A Compact ENDF (ACE) Format Specification," 2019.
- [10] "OECD Nuclear Energy Agency (NEA)," 2020. [Online]. Available: https://www.oecd-neo.org/jcms/pl_20505/evaluated-nuclear-data-library-descriptions#JEFF-FY.
- [11] J. Leppänen, Serpent – a Continuous-energy Monte Carlo Reactor Physics Burnup Calculation Code, 2015.
- [12] S. Wiki, "Delta and surface-tracking," 29 November 2017. [Online]. Available: https://serpent.vtt.fi/mediawiki/index.php/Delta-_and_surface-tracking.
- [13] O. Takuya, A. Yamamoto and E. Tomohiro, "An efficient execution of Monte Carlo simulation based on delta-tracking method using GPUs," 2017.
- [14] J. Leppänen, "Performance of Woodcock delta-tracking in lattice physics applications using the Serpent Monte Carlo reactor physics burnup calculation

code," vol. 37, pp. 715-722.

- [15] J. S. Rehaka, L. M. Kerby, M. D. DeHart and R. N. Slaybaugh, "Weighted Delta-Tracking in Scattering Media," 2018.
- [16] U. o. M. Amherst, "Lecture 17: The Law of Large Numbers and the Monte-Carlo method".
- [17] B. Rearden, SCALE Code System, Version 6.2.3 ed., M. Jessee, Ed., Office of Scientific and Technical Information PO Box 62 Oak Ridge, TN 37831, March 2018.
- [18] P. K. Romano, N. E. Horelik, B. R. Herman, A. G. Nelson, B. Forget and K. Smith, "OpenMC: A state-of-the-art Monte Carlo code for research and development," *Annals of Nuclear Energy*, vol. 82, pp. 90-97, 2015.
- [19] T. Kai, F. Maekawa and K. Kosako, "CHAIN-SP2001: high energy particle induced radioactivity calculation code," Tokai, 2001.
- [20] T. Sato, Y. Iwamoto, S. Hashimoto, T. Ogawa, T. Furuta, S.-i. Abe, T. Kai, P.-E. Tsai, N. Matsuda, H. Iwase, N. Shigyo, L. Sihver and K. Niita, "Features of Particle and Heavy Ion Transport codeSystem (PHITS) version 3.02," InformaUK Limited, trading as Taylor & FrancisGroup, 05 Jan 2018.
- [21] E. Brun, F. Damian, C. Diop, E. Dumonteil, F. Hugot, C. Jouanne, Y. Lee, F. Malvagi, A. Mazzolo, O. Petit, J. Trama, T. Visonneau and A. Zoia, "TRIPOLI-4®, CEA, EDF and AREVA reference Monte Carlo code," *Annals of Nuclear Energy*, vol. 82, pp. 151-160, 2015.
- [22] R. G. Sargent, "VERIFICATION AND VALIDATION OF SIMULATION MODELS," NY 13244, U.S.A. , 2011.
- [23] S. John and Carson, "MODEL VERIFICATION AND VALIDATION," GA 30067, U.S.A., 2002.
- [24] M. Chadwick, M. Herman, P. Obložinský, M. Dunn, A. K. Y. Danon, D. Smith, B. Pritychenko, G. Arbanas, R. Arcilla, R. Brewer, D. Brown, R. Capote, A. Carlson, Y. Cho, H. Derrien, K. Guber, G. Hale, S. Hoblit, S. Holloway and T. Johnson, "ENDF/B-VII.1 Nuclear Data for Science and Technology: Cross Sections, Covariances, Fission Product Yields and Decay Data," 2011.
- [25] NuclearPower, "Boron 10," 2021. [Online]. Available: <https://www.nuclear-power.com/glossary/boron-10/>.
- [26] W. J. Grantham, "BARYTES CONCRETE FOR RADIATION SHIELDING: MIX

CRITERIA AND ATTENUATION CHARACTERISTICS," United States, 1961.

- [27] Nagaya, Yasunobu, Chiba, Go, Mori, Takamasa, Irwanto, Dwi, Nakajima and Ken, "Comparison of Monte Carlo calculation methods for effective delayed neutron fraction," *Annals of Nuclear Energy*, Oxford, 2010.
- [28] T. Kaltiaisenaho, "Statistical Tests and the Underestimation of Variance in Serpent 2," 2014.
- [29] P. Saracco, S. Dulla and P. Ravetto, "The adjoint neutron transport equation and the statistical approach for its solution," 2016.
- [30] G. Chiba, Y. Nagaya and T. Mori, "On Effective Delayed Neutron Fraction Calculations with Iterated Fission Probability," *Journal of Nuclear Science and Technology*, pp. 1163-1169, 2011.
- [31] M. Stacey Weston, *Nuclear Reactor Physics, Second Edition, Completely Revised and Enlarged ed.*, Atlanta, USA: Georgia Institute of Technology Nuclear & Radiological Engineering, 2007.
- [32] D. Irwanto, T. Obara, G. Chiba and Y. Nagaya, "Study on calculation methods for the effective delayed neutron fraction," JAEA-Research--2010-061, Japan, 2011.
- [33] E. Malambu and Mbala, "Characterisation of neutron fields in support to dosimetry measurements in the BR1 Reactor using MCNP/X code simulations," NSP, SCK CEN, Boeretang 200, BE-2400 Mol, Belgium, April, 2020.
- [34] J. J. & H. L. J. Duderstadt, *Nuclear-Reactor Analysis*, i. John Wiley & sons, Ed., In *Nuclear Reactor Analysis*, 1976.
- [35] L. Fiorito, "MYRRHA core design version 1.8 - presentation".
- [36] Y. Molla, OPENMC MODELING OF THE CRITICAL MYRRHA CONFIGURATION: AN EMPHASIS IN CROSS SECTION HOMOGENIZATION, LAPPEENRANTA-LAHTI UNIVERSITY OF TECHNOLOGY LUT, 2020.
- [37] R. Ochoa, M. Vázquez, F. Álvarez-Velarde, F. Martín-Fuertes, N. García-Herranz and D. Cuervo, "A comparative study of Monte Carlo-coupled depletion codes applied to a Sodium Fast Reactor design loaded with minor actinides," 2013.
- [38] H. Barale, Application of the SERPENT2 code to neutronic analyses of the MYRRHA core: a sensitivity approach, Politecnico di Torino, 2020.

- [39] Waltar and Reynolds, Fast breeder reactors, Pergamon Press, 1981.
- [40] V. Valtavirta, M. Aufiero and J. Leppänen, A Novel Temperature Sensitivity Calculation Methodology for the Serpent Monte Carlo Code, vol. 121, Transactions of the American Nuclear Society, 2019, p. 1469–1472.
- [41] G. Van Den Eynde, E. Malambu, A. Stankovskiy, R. Fernandez and P. Baeten, "An updated core design for the multi-purpose irradiation facility MYRRHA," 2015.
- [42] W. S. Yang, Fast reactor physics and computational methods. Nuclear Engineering and Technology, 2012, pp. 44(2), 177–198.
- [43] D. De Bruyn, D. Maes, L. Mansani and B. Giraud, "From myrrha to XT-ADS: The design evolution of an experimental ADS system," AccApp'07, 2007.
- [44] J. T. Goorley, M. R. James, T. E. Booth, F. B. Brown, J. S. Bull, L. J. Cox, J. W. Durkee, J. S. Elson, M. L. Fensin, R. A. Forster, J. S. Hendricks, H. G. Hughes, R. C. Johns, B. C. Kiedrowski, S. G. Mashnik, G. W. McKinney and D. Pelowitz, MCNP6 user's manual, Los Alamos National Laboratory, 765, 2013.
- [45] P. Romojaro, Nuclear data analyses for improving the safety of advanced lead-cooled reactors [UPM], 2019.
- [46] G. Bell and S. Glasstone, Nuclear Reactor Theory, Vols. 6, 637, 1970.
- [47] I. C. Gauld and J. C. Ryman, Nuclide Importance to Criticality Safety, Decay Heating, and Source Terms Related to Transport and Interim Storage of High-Burnup LWR Fuel, NUREG/CR-6700, Ed., 2001.
- [48] P. D'Hondt, H. Aït Abderrahim, P. Kupschus, E. Malambu, T. Aoust, P. Benoit, V. Sobolev, K. Van Tichelen, B. Arien, F. Vermeersch, Y. Jongen, S. Ternier and D. Vandeplasseche, "Pre-design of MYRRHA, A Multipurpose Accelerator Driven System for Research and Development," in *AIP Conference Proceedings*, 2003.
- [49] B. Boer, M. Verwerft, V. Sobolev, D. Lamberts, S. Keijers, R. Fernandez, W. Lowet and E. Malambu, Preliminary design of the MYRRHA driver fuel system (Revision 2), vol. 5151, SCK•CEN/3818218, 2016.
- [50] N. S. Analysis, RELAP5/MOD3.3 code manual Volume I: Code Structure, System Models, and Solution Methods, NUREG/CR-5535/Rev P3-Vol I, 2003.
- [51] E. Malambu and A. Stankovskiy, Revised Core Design for MYRRHA-Rev1, SCK•CEN/3958903, 2014.

- [52] A. Borella, A. Calleja and L. Fiorito, Sensitivity studies on the production of Cm isotopes in spent fuel for safeguard applications. M&C 2017, International Conference on Mathematics & Computational Methods Applied to Nuclear Science & Engineering, 2017.
- [53] J. Wagemans, G. Vittiglio, E. Malambu and H. A. Abderrahim, "The BR1 Reactor: a Versatile Irradiation Facility for Fundamental Research and Industrial Applications," 2009.
- [54] R. L. Murray and K. E. Holbert, "Time Dependent Reactor Behavior. In Nuclear Energy," Elsevier, 2020.